Check for updates

AGU ADVANCING EARTH AND SPACE SCIENCES

Paleoceanography and Paleoclimatology

RESEARCH ARTICLE
10.1029/2024PA004856

# Orbital-Scale Global Ocean Sea Surface Temperatures Coupling With Cryosphere-Carbon Cycle Changes Over the Past 4 Million Years

**Ze Zhang[1], Eelco J. Rohling[2,3], David B. Kemp[4], Zhixiang Wang[5], and Chunju Huang[4]**

[1]Department of Atmospheric Science, School of Environmental Studies, China University of Geosciences, Wuhan, China, [2]Department of Earth Sciences, Utrecht University, Utrecht, The Netherlands, [3]Ocean and Earth Science, University of Southampton, National Oceanography Centre, Southampton, UK, [4]State Key Laboratory of Biogeology and Environmental Geology and Hubei Key Laboratory of Critical Zone Evolution, School of Earth Sciences, China University of Geosciences, Wuhan, China, [5]Qinghai Provincial Key Laboratory of Geology and Environment of Salt Lakes, Qinghai Institute of Salt Lakes, Chinese Academy of Sciences, Xining, China

**Key Points:**

- Orbital forcing of global sea surface temperatures (SST) evolution
- Enhancement of the obliquity signal in the global SSTs at ∼2.7 Ma is closely associated with the NH glaciation
- Changes in SST may drive processes of ocean-atmosphere carbon exchange that alter atmospheric $CO_2$ concentrations

**Supporting Information:**

Supporting Information may be found in the online version of this article.

**Correspondence to:**

Z. Wang and C. Huang,
wangzhi8905@126.com;
huangcj@cug.edu.cn

**Citation:**

Zhang, Z., Rohling, E. J., Kemp, D. B., Wang, Z., & Huang, C. (2024). Orbital-scale global ocean sea surface temperatures coupling with cryosphere-carbon cycle changes over the past 4 million years. *Paleoceanography and Paleoclimatology*, *39*, e2024PA004856. https://doi.org/10.1029/2024PA004856

Received 1 FEB 2024
Accepted 15 JUL 2024

**Author Contributions:**

**Conceptualization:** Ze Zhang, Eelco J. Rohling, Chunju Huang
**Data curation:** Ze Zhang
**Formal analysis:** Ze Zhang, Eelco J. Rohling, David B. Kemp, Zhixiang Wang
**Funding acquisition:** David B. Kemp, Chunju Huang
**Investigation:** Ze Zhang
**Methodology:** Ze Zhang, Eelco J. Rohling, David B. Kemp, Zhixiang Wang
**Project administration:** Chunju Huang
**Resources:** Zhixiang Wang
**Software:** Ze Zhang, Zhixiang Wang
**Supervision:** Eelco J. Rohling, David B. Kemp, Chunju Huang
**Validation:** David B. Kemp
**Visualization:** Ze Zhang
**Writing – original draft:** Ze Zhang
**Writing – review & editing:** Eelco J. Rohling, David B. Kemp, Zhixiang Wang, Chunju Huang

© 2024. American Geophysical Union. All Rights Reserved.

**Abstract** Changes in the thermal conditions of the ocean surface, the interface for air-sea exchange, are critical for understanding global climate and environmental change. Here we explore the evolution of sea surface temperature (SST) and the meridional SST gradient (STG) at orbital timescales since 4 million years ago (Ma), along with interactions between SSTs, the cryosphere, and the global carbon cycle. We observe orbital eccentricity and obliquity influences on SST evolution and infer that SST changes may have played a key role in atmospheric $CO_2$ and cryosphere changes through key climate transitions in the past 4 Ma. We find a major equator-to-pole STG increase in the Northern Hemisphere (NH) close to the initiation of major NH glaciation (at ∼2.7 Ma). In addition, we find substantial increases in the obliquity sensitivity ($S_{obl}$) of NH STG at ∼2.7 Ma and in Southern Hemisphere (SH) STG at ∼1 Ma, which may be responses to important expansions of NH and SH ice sheets, respectively. Phase analysis shows that SST changes typically lead global ice volume changes throughout the last 4 Ma. SST changes also lead atmospheric $CO_2$ changes since ∼1.5 Ma, which indicates that SST changes either drove, or directly reflect, processes that changed ocean-atmosphere carbon exchange and, thus, atmospheric $CO_2$ concentrations. Overall, our study emphasizes that SST changes were a critical component of climate change throughout the last 4 Ma.

**Plain Language Summary** A compilation of global sea surface temperature (SST) records indicates that SST mainly fluctuated on orbital eccentricity and obliquity timescales during the last 4 million years. The compilation also reveals an important impact of meridional ocean circulation changes on global climate since 4 Ma, with a particularly notable change in the equator-to-pole SST gradient during the initiation of major Northern Hemisphere glaciations at ∼2.7 Ma. Finally, we find that SST changes played a key role in the atmospheric $CO_2$ changes associated with global climate transformations.

## 1. Introduction

The oceans play a fundamental role in the climate system due to their enormous heat-storage capacity (Deser et al., 2010), and sea surface temperature (SST) changes since the early Pliocene are thought to have been a potential cause of the onset of NH glacial cycles (Fedorov et al., 2013). In addition, SST evolution profoundly affects atmospheric circulation patterns (Brierley et al., 2009; Fedorov et al., 2013), as the ocean can transfer energy to the atmosphere through turbulence and radiative energy exchange at the sea surface (Deser et al., 2010). As such, SST assessment is crucial for understanding the evolution of Earth's climate system and the mechanisms of climate change. The emergence of increasing numbers of SST records based on geochemical proxies, such as the alkenone unsaturation index ($U^{K'}_{37}$) and foraminiferal Mg/Ca ratios, has greatly improved understanding of global long-term SST evolution since the Pliocene (Lawrence et al., 2006, 2009; Liu & Herbert, 2004; Max et al., 2020; O'Brien et al., 2014). However, it remains unclear how SST affects other climate processes under changing geological boundary conditions, such as different atmospheric $CO_2$ concentrations (Fedorov et al., 2015).

The temperature of the ocean surface, the interface of air-sea exchange, is controlled by a combination of atmospheric and oceanic processes. The air-sea temperature contrast and wind velocity dominate air-sea heat exchange, mainly in the form of latent and sensible heat (Cayan, 1992). Ocean circulation (Dowsett et al., 2009),

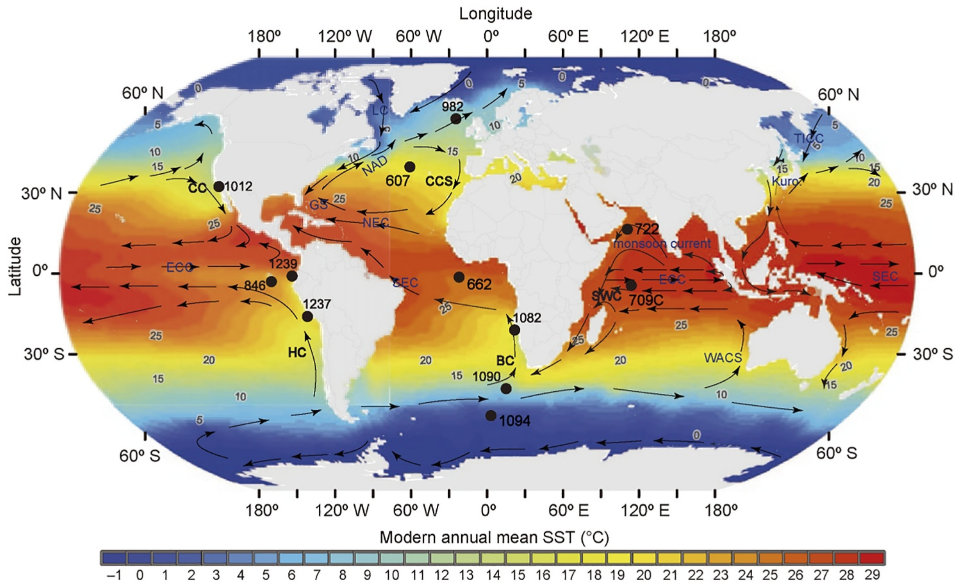


**Figure 1.** Map of sites (black dots) from which data were retrieved (data are from: Brierley et al., 2009; Dekens et al., 2007; Etourneau et al., 2009, 2010; Hasenfratz et al., 2019; Herbert et al., 2010; Karas et al., 2011; Lawrence et al., 2006, 2009, 2010; Liu & Herbert, 2004; Martínez-Garcia et al., 2010), superimposed on a map of modern annual mean sea surface temperature (contours and colors after Fedorov et al., 2013). Numbers indicate sites from the Deep Sea Drilling Project (DSDP), the Ocean Drilling Program (ODP), the Integrated ODP and International Ocean Discovery Program (both IODP), and the International Marine Global Change Study (IMAGES). Black arrows indicate modern global ocean circulation. Acronyms: Atlantic Drift (NAD), Gulf Stream (GS), North Equatorial Current (NEC), South Equatorial Current (SEC), Humboldt Current (HC), Labrador Current (LC), California Current (CC), Equatorial Counter Current (ECC), Thousand Islands Cold Current (TICC), Kuroshio (Kuro.), Canary Cold Stream (CCS), Benguela Current (BC), Somali Warm Current (SWC), and Western Australian Cold Stream (WACS).

vertical mixing (Hasenfratz et al., 2019), and thermocline depth (Wara et al., 2005) also significantly affect SST. SST records from different latitudes (Figure 1) show large-scale variations with time similar to those in records of the oxygen isotope composition of benthic foraminifera ($\delta^{18}O_{benthic}$) and atmospheric $CO_2$ concentrations, but substantial differences exist at more detailed levels (Figure 2). $\delta^{18}O_{benthic}$ is a well-established proxy for the evolution of deep-sea temperatures and seawater $\delta^{18}O$ ($\delta^{18}O_{sw}$), the latter of which is related to global ice volume (De Vleeschouwer et al., 2020; Fedorov et al., 2013; Rohling et al., 2021). Hence, similarities between large-scale variations in $\delta^{18}O_{benthic}$ and SST reflect the global nature of glacial-interglacial cycles, while differences reflect leads, lags, and amplitude response differences that may hold clues about the nature of the processes by which they are connected.

Here we focus on three issues that remain poorly explored within the past 4 million years, namely: (a) global-scale SST evolution at orbital time scales, (b) the evolution of the meridional SST gradient (STG) between the tropics, extra-tropics, and polar regions, and (c) the relationships between SST, global ice volume, and atmospheric $CO_2$. We investigate the role of meridional ocean circulation changes in some of the major climate events of the last 4 Myr. The first event concerns the initiation of major NH glaciation (NHG) during the Late Pliocene-Early Pleistocene (LP/EP, ∼3–2.7 Ma), when the NH transitioned from warm, virtually ice-free climatic conditions to a cold, persistent ice age climate, marked by an emerging dominance of 41-kyr obliquity cycles in $\delta^{18}O_{benthic}$ records (Lisiecki & Raymo, 2005; Westerhold et al., 2020). The second event concerns the mid-Pleistocene transition (MPT, ∼1.2–0.7 Ma), when dominant 41-kyr obliquity cycles gave way to high-amplitude 100-kyr eccentricity cycles in $\delta^{18}O_{benthic}$ records (Lisiecki & Raymo, 2005; Raymo et al., 2006; Westerhold et al., 2020).

## 2. Materials and Methods

### 2.1. Data Sources

The International Ocean Discovery Program (IODP) and its predecessors have provided the high-quality sediment sequences used in the generation of a valuable set of Cenozoic climate and SST. We use alkenone



25724525, 2024, 7, Downloaded from https://agupubs.onlinelibrary.wiley.com/doi/10.1029/2024PA004856 by University Of Southampton, Wiley Online Library on [25/07/2024]. See the Terms and Conditions (https://onlinelibrary.wiley.com/terms-and-conditions) on Wiley Online Library for rules of use; OA articles are governed by the applicable Creative Commons License

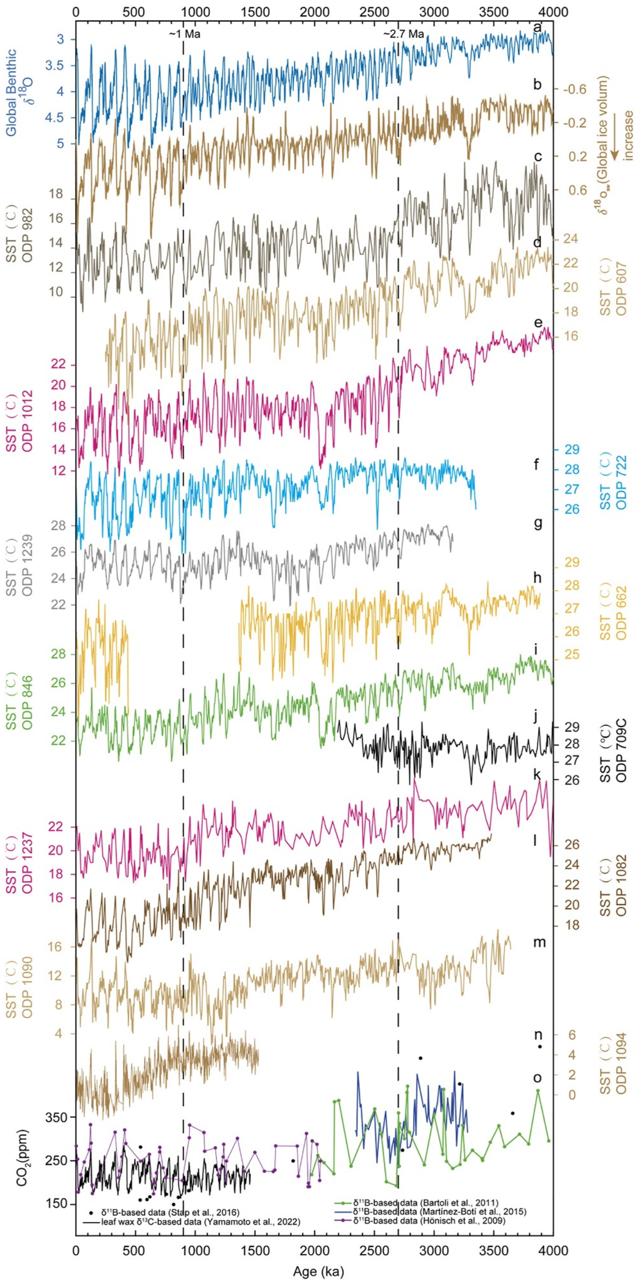


**Figure 2.** Sea surface temperature (SST) and $CO_2$ concentration records shown with benthic foraminiferal $\delta^{18}O$ and seawater $\delta^{18}O_{sw}$ for the past 4,000 kyr (4 Myr). (a) Benthic foraminiferal $\delta^{18}O$ (LR04 stack; Lisiecki & Raymo, 2005). (b) Seawater $\delta^{18}O_{sw}$ (proxy for global ice volume; Rohling et al., 2021). The direction of the arrow indicates increasing ice volume. (c) SST of ocean drilling program (ODP) Sites 982 (North Atlantic; Lawrence et al., 2009). (d) SST of deep sea drilling project Site 607 (North Atlantic; Lawrence et al., 2010). (e) SST of ODP Site 1012 (North Pacific; Brierley et al., 2009). (f) SST of ODP Site 722 (Arabian Sea; Herbert et al., 2010). (g) SST of ODP Site 1239 (Eastern equatorial Pacific; Etourneau et al., 2010). (h) SST of ODP Site 662 (Equatorial Atlantic; Herbert et al., 2010). (i) SST of ODP Site 846 (Eastern equatorial Pacific; Lawrence et al., 2006; Liu & Herbert, 2004). (j) SST of ODP Site 709°C (Indian Ocean; Karas et al., 2011). (k) SST of ODP Site 1237 (South Pacific; Dekens et al., 2007). (l) SST of ODP Site 1082 (South Atlantic; Etourneau et al., 2009). (m) SST of ODP Site 1090 (Subantarctic; Martínez-Garcia et al., 2010). (n) SST of ODP Site 1094 (Antarctic; Hasenfratz et al., 2019). (o) Estimated atmospheric $CO_2$ concentrations (Bartoli et al., 2011; Hönisch et al., 2009; Martínez-Botí et al., 2015; Stap et al., 2016; Yamamoto et al., 2022).



25724525, 2024, 7, Downloaded from https://agupubs.onlinelibrary.wiley.com/doi/10.1029/2024PA004856 by University Of Southampton, Wiley Online Library on [25/07/2024]. See the Terms and Conditions (https://onlinelibrary.wiley.com/terms-and-conditions) on Wiley Online Library for rules of use; OA articles are governed by the applicable Creative Commons License

25724525, 2024, 7, Downloaded from https://agupubs.onlinelibrary.wiley.com/doi/10.1029/2024PA004856 by University Of Southampton, Wiley Online Library on [25/07/2024]. See the Terms and Conditions (https://onlinelibrary.wiley.com/terms-and-conditions) on Wiley Online Library for rules of use; OA articles are governed by the applicable Creative Commons License

unsaturation index ($U^{K'}_{37}$) based SST records for Site 982 from the North Atlantic (58°N, 16°W; Lawrence et al., 2009), Site 607 from the North Atlantic (41°N, 33°W; Lawrence et al., 2010), Site 1012 from the North Pacific (32°N, 118°W; Brierley et al., 2009), Site 722 from the Arabian Sea (16.6°N, 59.8°W; Herbert et al., 2010), Site 846 (3°S, 91°W; Lawrence et al., 2006; Liu & Herbert, 2004), Site 1239 (1°S, 82°W; Etourneau et al., 2010) from the Equatorial Pacific, Site 662 from the Equatorial Atlantic (1°S, 12°W; Herbert et al., 2010), Site 709°C from the Indian Ocean (3°54.9′S, 60°33.1′E; Karas et al., 2011), Site 1237 from the South Pacific (16°S, 76°W; Dekens et al., 2007), Site 1082 (21°S, 12°E; Etourneau et al., 2009) from the Southern Ocean, Site 1090 (43°S, 9°E; Martínez-Garcia et al., 2010) from the Subantarctic, and Site 1094 (53.2°S, 5.1°E; Hasenfratz et al., 2019) from the Antarctic Zone. The age models for the sites used in this study, with exception of Site 1237, are based on orbital tuning of deep-sea oxygen isotope records (LR04 stack; Lisiecki & Raymo, 2005; see Table S1 in Supporting Information S1 for details). The $U^{K'}_{37}$ index and foraminiferal Mg/Ca are widely used to reconstruct ocean temperatures. Use of the $U^{K'}_{37}$ proxy is limited in warm tropical regions, where the $U^{K'}_{37}$ index can saturate at temperatures >29°C (Fedorov et al., 2013; Li et al., 2011). We include $U^{K'}_{37}$ based SSTs for three tropical sites (Sites 662, 846 and 1239; Figure S1 in Supporting Information S1), given that values remained below that 29°C limit (Figure S1 in Supporting Information S1).

Atmospheric $CO_2$ concentrations are obtained from reconstructions based on leaf wax $\delta^{13}C$ at IODP Site U1446 (0–1.46 Ma; Yamamoto et al., 2022) and foraminiferal $\delta^{11}B$ (0–4 Ma; Figure 2o; Bartoli et al., 2011; Hönisch et al., 2009; Martínez-Botí et al., 2015; Stap et al., 2016). The IODP Site U1446 leaf wax $\delta^{13}C$ record has a resolution of ~1.7 kyr, which we use for orbital-scale phase analysis. Its age model is derived from oxygen isotope tuning to the global $\delta^{18}O_{benthic}$ (LR04) stack by Clemens et al. (2021). The $\delta^{18}O_{sw}$ record in Figure 2b has been derived from the CENOGRID $\delta^{18}O_{benthic}$ record of Westerhold et al. (2020) by Rohling et al. (2021), and has a 1 kyr resolution. The resolution of the collated data sets makes them suitable for analyzing changes in Earth's climate system at orbital time scales.

Meridional SST gradients (STG) are created by calculating the difference in SSTs between 2 ocean cores from different latitudes in the same ocean. For this study, we take these calculated STGs to be representative of the basin-wide situation as suggested by previous studies (Brierley et al., 2009; Wara et al., 2005). Due to differences between the temporal resolutions of the different SST records, we interpolated SST records from the different sites to 2 kyr spacing and then calculated the gradients. The North Atlantic STG is determined between ocean drilling program (ODP) sites 982 and 662; the North Pacific STG is that between ODP Sites 846 and 1012; the South Atlantic STG uses ODP sites 1082 and 1090; and the South Pacific STG is the difference between ODP Sites 1239 and 1237.

### 2.2. Spectral Analysis

SST power spectra and sliding window spectrograms were calculated using Acycle 2.6 (Li et al., 2019). All records were detrended by fitting and removing LOESS functions (35%). SST power spectra were analyzed using the 2π-MultiTaper Method (MTM) with robust red noise modeling to ascertain 95% confidence levels. Eccentricity and obliquity cycles in the SST records were extracted using Gaussian band-pass filtering in Acycle 2.6 (Li et al., 2019).

### 2.3. Obliquity Sensitivity

Obliquity sensitivity ($S_{obl}$) is calculated as $\sigma^2_{STG}/\sigma^2_{La04}$, where $\sigma^2_{STG}$ is the temporal variance of obliquity in the STG in units of °$C^2$, and $\sigma^2_{La04}$ is the temporal variance of obliquity in units of degrees$^2$, taken from the Laskar et al. (2004) orbital solution (La04). Obliquity variance was quantified using multitaper time-frequency power spectra by integrating the variance between 0.023 and 0.027 cycles/kyr (i.e., from ~43.5 to 37 kyr). All time-frequency analyses were performed using three 2π prolate data tapers, with a 400-kyr window and a 10-kyr time step. The analysis was carried out in *R* and the *R* code was modified after Levy et al. (2019).

### 2.4. Phase Analysis

SST-$\delta^{18}O_{sw}$ and SST-$CO_2$ phase relationships were calculated using cross-spectral analysis in the IRISSeismic package in *R* (Callahan et al., 2018). To visualize results, we invert $\delta^{18}O_{sw}$ to make it positively correlated with sea level. Our study focuses on phase relationships between SST, $\delta^{18}O_{sw}$, and $CO_2$ on eccentricity scales. We calculated cross spectra using a 400-kyr sliding window and a 10-kyr step size in individual data sets. Phase analysis calculated at the ~100-kyr eccentricity scale was chosen for a 90–135 kyr period range with the highest

25724525, 2024, 7, Downloaded from https://agupubs.onlinelibrary.wiley.com/doi/10.1029/2024PA004856 by University Of Southampton, Wiley Online Library on [25/07/2024]. See the Terms and Conditions (https://onlinelibrary.wiley.com/terms-and-conditions) on Wiley Online Library for rules of use; OA articles are governed by the applicable Creative Commons License

period coherence. The phase analysis was carried out in *R* and the *R* code was modified after De Vleeschouwer et al. (2020).

### 2.5. Recurrence Analysis

Non-linear structure within proxy time series can help to reveal regime/system changes that cannot be validated otherwise by visual inspection or linear methods like spectral analysis (Han et al., 2020; Marwan et al., 2007). Recurrence analysis is used to identify transitions between different types of dynamics within a time series. Recurrence plots are matrix plots that visualize a fundamental property of dynamical systems–namely, when a system "repeats" itself, returning to a previous state (See Text S1 in Supporting Information S1 for a detailed description). Recurrence plots are a binary matrix where the coordinates of each entry mark the pair of time points with recurring states (Marwan et al., 2007). If climate dynamics have consistent patterns, they will show up as darker areas in the plot; if they have no common dynamics, the plot will remain white (Marwan et al., 2007; Westerhold et al., 2020). We conducted recurrence analyses of non-detrended SST data in Matlab's CRP Toolbox (Marwan, 2020).

## 3. Results and Discussion

### 3.1. Combined High- and Low-Latitude Forcing of Regional SSTs Since 4 Ma

There is a strong statistical relationship between $U^{K'}_{37}$ and mean annual SST in many regions (Müller et al., 1998; Rosell-Melé, 1998); hence its use as an SST proxy. However, many studies have shown that coccolithophorid productivity (i.e., the main source of alkenone) is highest in subpolar ocean regions during the summer to autumn months (Lawrence et al., 2009; Max et al., 2020; Samtleben & Bickert, 1990). A study on coccolithophore fluxes in the Bering Sea and subpolar Pacific (Tsutsui et al., 2016) has further demonstrated that the main blooming season and export of coccolithophores is heavily biased to October–November. Despite the potential seasonal bias in the $U^{K'}_{37}$ proxy implicit in these studies, other work has suggested that alkenone production may have been much less seasonal in the warm early Pliocene (Lawrence et al., 2009). Overall, there is potential for the SSTs reconstructed from the $U^{K'}_{37}$ index to be biased. Our analyses provide some perspective on this, as follows.

Our analyses highlight prominent eccentricity (both 400-kyr and 100-kyr) cycles in SST records in both low and mid-latitude, and high-latitude oceans since 4 Ma (Figures 3–5; Figures S2, S3 in Supporting Information S1), and this strong eccentricity cycle is also present in SST records reconstructed using foraminiferal Mg/Ca (Site 709°C and 1094, Figures 4d and 5d). The eccentricity cycles in SST records are consistent with theoretical eccentricity cycles (Figure S3 in Supporting Information S1). Yet, annual mean insolation variability at the various sites is almost entirely dominated by obliquity, and the direct impact of eccentricity is very weak (Figure S4 in Supporting Information S1). This agrees with obliquity cycle influences on insolation (Laskar et al., 2004) and relatively negligible direct contributions of eccentricity to insolation changes (<0.1%) (Clemens & Tiedemann, 1997). However, eccentricity still modulates the amplitude of precession impacts, which controls the amount of summer insolation (e.g., equatorial Pacific planktonic foraminiferal Mg/Ca-based SSTs show dominant precession variability since 140 ka; Jian et al., 2020). This, with additional carbon cycle changes and ice-albedo effects (Pälike et al., 2006), can drive major temperature responses at low latitudes (De Boer et al., 2014; Liebrand et al., 2017; Westerhold et al., 2020). Coupling between eccentricity pacing and carbon cycle variations has been inferred throughout the late Neogene based on carbon isotope variations (De Vleeschouwer et al., 2020), and is apparent also from orbital-scale covariation between global SST and atmospheric $CO_2$ concentrations (Figure 2) (also Liebrand et al., 2017; Pälike et al., 2006). We infer that whatever is measured by the $U^{K'}_{37}$ index (either annual mean SSTs, or summer and autumn SSTs) reflects predominantly precession-based summer-insolation control, where persistence of insolation-driven summer and autumn warming affects winter SSTs due to the great thermal capacity of ocean water. Our observed prominence of eccentricity variability then reflects longer-term amplitude modulation of such precession influences.

Sliding window spectrograms of SSTs in the NH and equatorial regions reveal strong obliquity (41-kyr) variability between ∼2.7 and ∼0.7 Ma (except at Site 846; Figures 3 and 4; see also Figure S5 in Supporting Information S1). Although our collection of SST records from three Southern Hemisphere sites do not show a change in the obliquity signal during the Late Pliocene, a recent Southern Hemisphere SST stack that integrates additional records reveals substantial significant obliquity enhancement around 2.7 Ma (Clark et al., 2024). Our

10.1029/2024PA004856

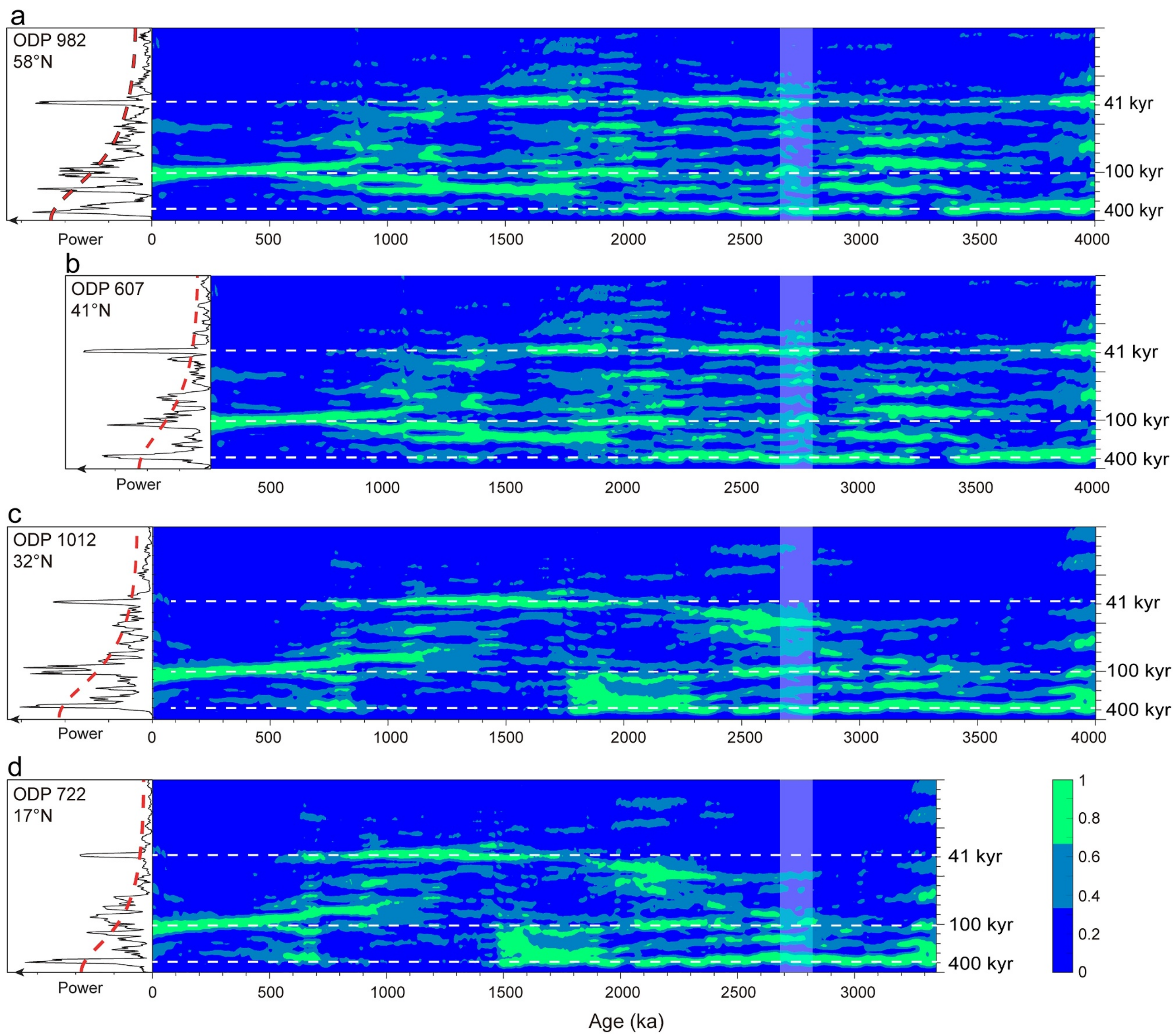


**Figure 3.** Astronomical evolution of SSTs from ocean drilling sites at different latitudes in the Northern Hemisphere. Spectrograms with 600 kyr sliding windows with 2π multi-taper (MTM) power spectra of (a) sea surface temperature (SST) of ocean drilling program (ODP) Site 982 since 4 Ma, (b) SST of deep sea drilling project Site 607 since 4 Ma, (c) SST of ODP Site 1012 since 4 Ma, (d) SST of ODP Site 722 since ∼3.3 Ma. SSTs from these sites were reconstructed using $U^{K'}_{37}$. The red dotted lines on the power spectra are the 95% confidence levels. The arrows on the power *x*-axes indicate the enhancement of the periodic signal in the spectrogram. The colors in the sliding window spectrogram indicate the strength of the periodic signal, with blue-grayish blue-green indicating an increasingly strong periodic signal. The white shaded band indicates the enhancement of the obliquity signal at ∼2.7 Ma.

spectral analysis of the global SST stack from the same publication shows that this enhancement of the obliquity signal at ∼2.7 Ma is global in nature (Figure S6 in Supporting Information S1).

Obliquity signals at high latitudes are commonly interpreted in terms of annual mean solar radiation variations (Bosmans et al., 2015; Naish et al., 2009), but the reasons for weaker obliquity before ∼2.7 Ma and after ∼0.7 Ma are uncertain. At low latitudes, the proportional impact of obliquity on annual mean insolation is relatively small (cf. spatio-temporal illustrations in Loutre et al., 2004; Rohling et al., 2012), but we still observe a marked obliquity signal in tropical SST records between ∼2.7 and ∼0.7 Ma (Figure 4). Obliquity signals have also been found after ∼2.7 Ma in other low latitude records (e.g., Lourens et al., 2001). Some studies have suggested ocean circulation as a possible mechanism for transfer of high-latitude obliquity influences to lower latitudes (Jouzel et al., 2007). Other studies have suggested that interhemispheric temperature gradients may be critical (Bosmans et al., 2015; Li et al., 2017; Raymo & Nisancioglu, 2003). Meridional temperature gradients drive both



25724525, 2024, 7, Downloaded from https://agupubs.onlinelibrary.wiley.com/doi/10.1029/2024PA004856 by University Of Southampton, Wiley Online Library on [25/07/2024]. See the Terms and Conditions (https://onlinelibrary.wiley.com/terms-and-conditions) on Wiley Online Library for rules of use; OA articles are governed by the applicable Creative Commons License

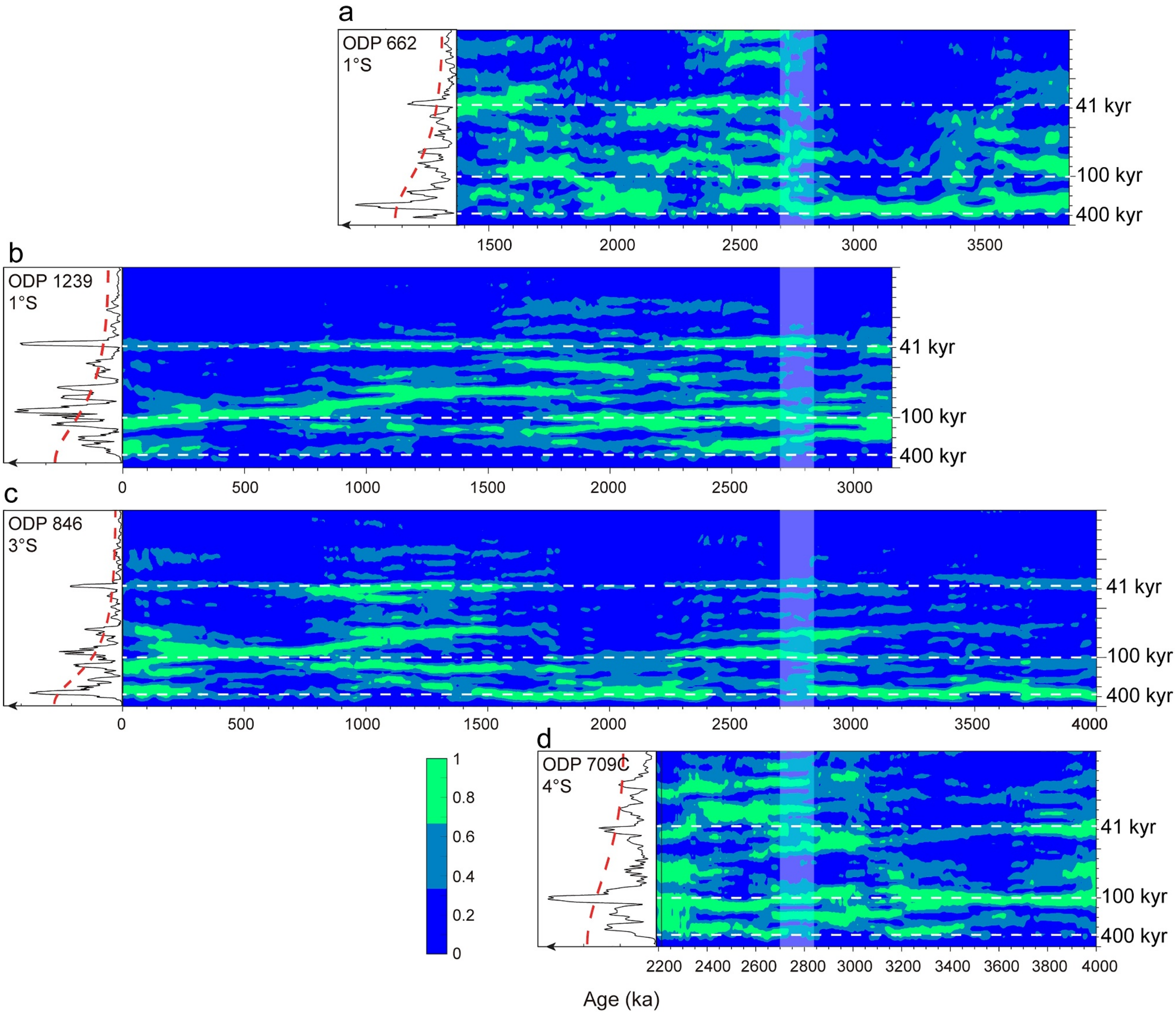


**Figure 4.** Astronomical evolution of sea surface temperature (SST) from ocean drilling sites in the equatorial region. Spectrograms with 600 kyr sliding windows with 2π multi-taper (MTM) power spectra of (a) SST of ocean drilling program (ODP) Site 662 since 4 Ma, (b) SST of ODP Site 1239 since 4 Ma, (c) SST of ODP Site 846 since ~3.9 Ma, (d) SST of ODP Site 709°C from ~4.9 to ~2.2 Ma. SST of ODP Sites 709°C were reconstructed using foraminiferal Mg/Ca, and the remaining SST temperatures were reconstructed using $U^{K'}_{37}$. The red dotted line on the power spectra are the 95% confidence levels. The arrows on the power *x*-axes indicate the enhancement of the periodic signal in the spectrogram. The colors in the sliding window spectrogram indicate the strength of the periodic signal, with blue-grayish blue-green indicating an increasingly strong periodic signal. The white shaded band indicates the enhancement of the obliquity signal at ~2.7 Ma.

atmospheric heat and moisture transport toward the poles (Brierley & Fedorov, 2010; Fedorov et al., 2013; Raymo & Nisancioglu, 2003). However, the hemispheric insolation gradient has not changed significantly since 4 Ma, and no consensus explanation has yet been reached for the abrupt appearance of the obliquity signal at that time, for its strength across the LP/EP, or for its weakness after the MPT (especially at low latitudes) (Kender et al., 2018; Raymo et al., 2006; Yehudai et al., 2021). The explanation must include a mechanism that amplifies the Earth system response to obliquity variations, including especially its unexpected predominance at low latitudes.

To investigate this issue, we calculate meridional SST gradients (STG) in the North Pacific, North Atlantic, South Pacific and South Atlantic (Figure 6). We also present a new assessment of STG sensitivity to obliquity forcing ($S_{obl}$), which represents the ratio of obliquity-band variance in STG to the variance in obliquity (Figure 6; see Section 2). Given that previous studies have demonstrated that the influence of obliquity-driven ocean dynamics changes is amplified when Antarctic or Northern Hemisphere ice sheets expand into the marine environment (Cao



25724525, 2024, 7, Downloaded from https://agupubs.onlinelibrary.wiley.com/doi/10.1029/2024PA004856 by University Of Southampton, Wiley Online Library on [25/07/2024]. See the Terms and Conditions (https://onlinelibrary.wiley.com/terms-and-conditions) on Wiley Online Library for rules of use; OA articles are governed by the applicable Creative Commons License

10.1029/2024PA004856

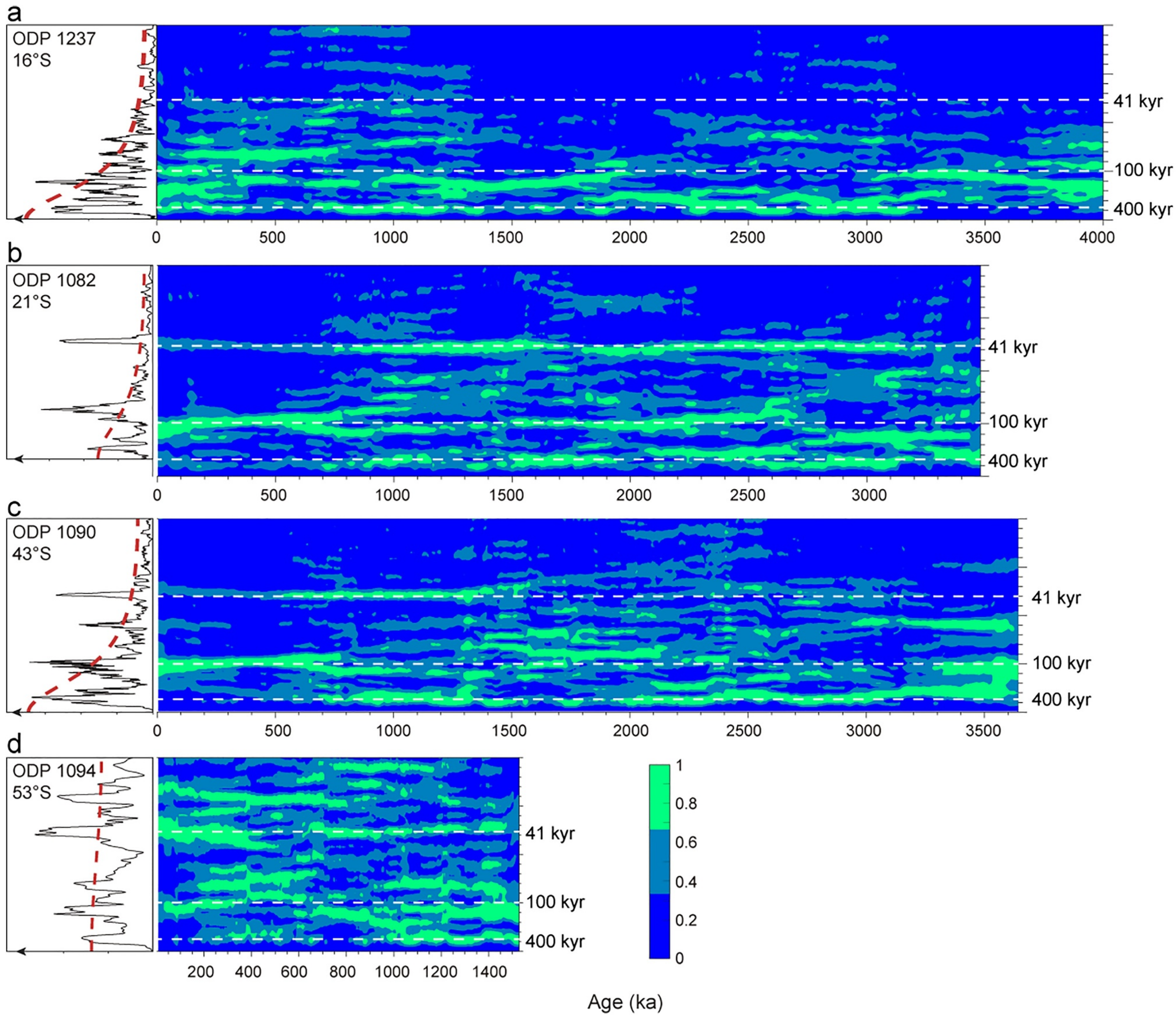


**Figure 5.** Astronomical evolution of sea surface temperature (SST) from ocean drilling sites at different latitudes in the Southern Hemisphere. Spectrograms with 600 kyr sliding windows with 2π multi-taper (MTM) power spectra of (a) SST of ocean drilling program (ODP) Site 1237 since 4 Ma, (b) SST of ODP Site 1082 since ~3.5 Ma, (c) SST of ODP Site 1090 since ~3.6 Ma, (d) SST of ODP Site 1094 from 1.5 to 0.9 Ma. ODP Sites 1094 were reconstructed using foraminiferal Mg/Ca, and the remaining SST temperatures were reconstructed using $U^{K'}_{37}$. Note that the absence of an obliquity signal in the SST record at ODP Site 1237 is likely due to this record's lower temporal resolution (~14 kyr). The red dotted line on the power spectra are the 95% confidence levels. The arrows on the power *x*-axes indicate the enhancement of the periodic signal in the spectrogram. The colors in the sliding window spectrogram indicate the strength of the periodic signal, with blue-grayish blue-green indicating an increasingly strong periodic signal.

et al., 2021; Levy et al., 2019), variations in $S_{obl}$ may reflect major changes in terrestrial versus marine-based ice sheet responses to obliquity forcing (Levy et al., 2019).

We find substantial $S_{obl}$ increases in NH STG records at ~2.7 Ma (Figures 6b and 6c), without noticeable $S_{obl}$ changes in SH STG records (Figures 6d and 6e). At the same time, the STG in the NH also increased significantly at ~2.7 Ma (Figures 6b and 6c). The ~2.7 Ma time interval marks the intensification of Northern Hemisphere glaciation (iNHG), which is recognized in climate proxy data that include deep-sea oxygen isotopes (Lisiecki & Raymo, 2005; Westerhold et al., 2020), North Atlantic planktonic foraminiferal assemblages (Dowsett & Poore, 1990) and ice rafted debris records (Smith et al., 2018). This suggests that the strong global expression of obliquity in SST records at ~2.7 Ma likely resulted from $S_{obl}$ increase associated with establishment of large-scale NH ice sheets. Conversely, a distinct $S_{obl}$ increase in SH STG records at ~1 Ma may reflect expansion of the East Antarctic ice sheet (EAIS) margin into the ocean (Raymo et al., 2006), which would result in an enhanced



25724525, 2024, 7, Downloaded from https://agupubs.onlinelibrary.wiley.com/doi/10.1029/2024PA004856 by University Of Southampton, Wiley Online Library on [25/07/2024]. See the Terms and Conditions (https://onlinelibrary.wiley.com/terms-and-conditions) on Wiley Online Library for rules of use; OA articles are governed by the applicable Creative Commons License

response to obliquity in the SH (Levy et al., 2019). EAIS expansion into the ocean at around this time agrees with drill core data that indicate widespread expansion of a marine-based ice sheet in the Ross Embayment at the MPT (McKay et al., 2012). A $S_{obl}$ decrease in the North Atlantic and North Pacific STGs at ∼2.4 Ma (Figures 6b and 6c) corresponds to a negative $\delta^{18}O_{sw}$ shift (Figure 6a), which suggests that a reduction in global ice volume led to a $S_{obl}$ decrease in the climate records.

### 3.2. Coupling Between SST, Carbon Cycle, and Cryospheric Changes Since 4 Ma

The causes of the iNHG at ∼2.7 Ma and subsequent frequency and amplitude changes of glacial cycles remain debated (Chalk et al., 2017; Kender et al., 2018; Willeit et al., 2019; Yehudai et al., 2021). Explanations for the LP/EP and MPT climate changes often invoke atmospheric $CO_2$ and ice volume variations as critical links between orbital forcing and the climate response (Willeit et al., 2019; Yehudai et al., 2021). Hence, we investigate relationships between SST, global ice volume ($\delta^{18}O_{sw}$), and atmospheric $CO_2$ concentrations using time-evolutive SST-$\delta^{18}O_{sw}$ and SST-$CO_2$ phase analysis on 100-kyr eccentricity timescales (90–135 kyr period range). We use 400-kyr-wide sliding windows and 10-kyr steps to calculate leads and lags between SST, $\delta^{18}O_{sw}$, and $CO_2$ concentrations (see Methods). We find that SST led $CO_2$ concentrations for most of the time since ∼1.5 Ma, with a lead of about 0–17 kyr (0–60°, Figure 7b) (ODP Sites 662, 709°C and 1237 were not used for phase analysis due to data discontinuities and their low temporal resolution). SST led global ice volume for most of the time since ∼4 Ma, with a lead time of about 0–28 kyr (0–100°). However, some sites show that ice volume led SST between 2.2 and 1.5 Ma. The phase difference at these times is relatively large (50–180°; 14–50 kyr), which may suggest a decoupling between ice volume and SST between 2.2 and 1.5 Ma (Figure 7a).

The persistent lead of SSTs over global $CO_2$ concentrations (since 1.5 Ma) and ice volume (since 4 Ma, except for 2.2–1.5 Ma) suggests that SST changes played an important role in global climate cycles since 4 Ma. We find that the phase difference between $CO_2$ and ice volume is smaller and more stable (0–25°; 0–7 kyr) than the phase difference between SST and ice volume (0–100°; 0–28 kyr), which suggests that $CO_2$ changes are more likely to be directly responsible for changes in global ice volume. This result could be informative also in the context of future climate change caused by anthropogenically forced increase in atmospheric $CO_2$. Reconstructed $CO_2$ data suggest a significant decrease from ∼2.7 Ma (Figure 2o), associated with the iNHG. Due to a lack of high-resolution atmospheric $CO_2$ reconstructions before 1.5 Ma, we have no way to determine phase relationships between $CO_2$, SST, and ice volume at ∼2.7 Ma. However, we find that SST has continued to lead atmospheric $CO_2$ since ∼1.5 Ma (Figure 7b; Figure S7 in Supporting Information S1). There is about 39,000 PgC of dissolved carbon stored in the oceans; more than 13 times the amount in the atmosphere and terrestrial biosphere combined (IPCC, 2007). Therefore, the mechanisms responsible for long-term changes in atmospheric $CO_2$ concentrations likely are ocean-related (Kohfeld & Ridgwell, 2009). Previous work has elucidated the importance of carbon redistribution between the atmosphere and ocean carbon reservoirs in driving atmospheric $CO_2$ changes, notably through $CO_2$ sequestration/release from the deep ocean (e.g., De Boer & Hogg, 2014; Hasenfratz et al., 2019; Kohfeld & Chase, 2017; Kohfeld & Ridgwell, 2009; Sigman et al., 2010; Yu, Anderson, & Rohling, 2014, Yu, Anderson, Jin, et al., 2014, 2016, 2019, 2020).

Explaining the large (>100 ppm) atmospheric $CO_2$ drops associated with glacials requires a complex set of interconnected oceanic processes, including: (a) direct dissolution of atmospheric $CO_2$ into seawater (Kohfeld & Ridgwell, 2009; Martin et al., 2005; Yu, Anderson, & Rohling, 2014); (b) enhanced ocean biological pump activity (Hain et al., 2014; Martínez-Garcia et al., 2011); (c) weakened deep-ocean circulation (Farmer et al., 2019; Pena & Goldstein, 2014); and (d) reduced $CO_2$ exchange between the deep sea and the surface ocean ("stratification"; Martin et al., 2005; Hasenfratz et al., 2019). Sequestered $CO_2$ becomes "trapped" in the deep sea, as confirmed by deep-sea [$CO_3^{2-}$] reconstructions (Anderson et al., 2008; Ridgwell & Zeebe, 2005; Yu et al., 2016, 2019, 2020). Air-sea disequilibrium can also enhance ocean carbon storage (Eggleston & Galbraith, 2018; Ito & Follows, 2013; Khatiwala et al., 2019; Odalen et al., 2018). In fact, previous studies in the Southern Ocean and the subarctic North Pacific based on biogenic opal accumulation and nitrogen isotope records indicate that a transition toward permanent polar ocean water-column stratification at ∼2.7 Ma may have been a key driver of the atmospheric $CO_2$ decline (Haug et al., 1999; Sigman et al., 2010). This polar ocean stratification is thought to have been controlled by both temperature and salinity changes (Sigman et al., 2004). Our compiled data set indicates that North Atlantic and North Pacific SSTs decreased markedly from 4 to ∼2.7 Ma (ODP Sites 982 and 607; Figures 2c and 2d), while the corresponding STG increased (Figures 6b and 6c). NH high latitude cooling (ODP Sites 982 and 1012, Figures 2c and 2e) would increase the equatorial-to-polar meridional



25724525, 2024, 7, Downloaded from https://agupubs.onlinelibrary.wiley.com/doi/10.1029/2024PA004856 by University Of Southampton, Wiley Online Library on [25/07/2024]. See the Terms and Conditions (https://onlinelibrary.wiley.com/terms-and-conditions) on Wiley Online Library for rules of use; OA articles are governed by the applicable Creative Commons License

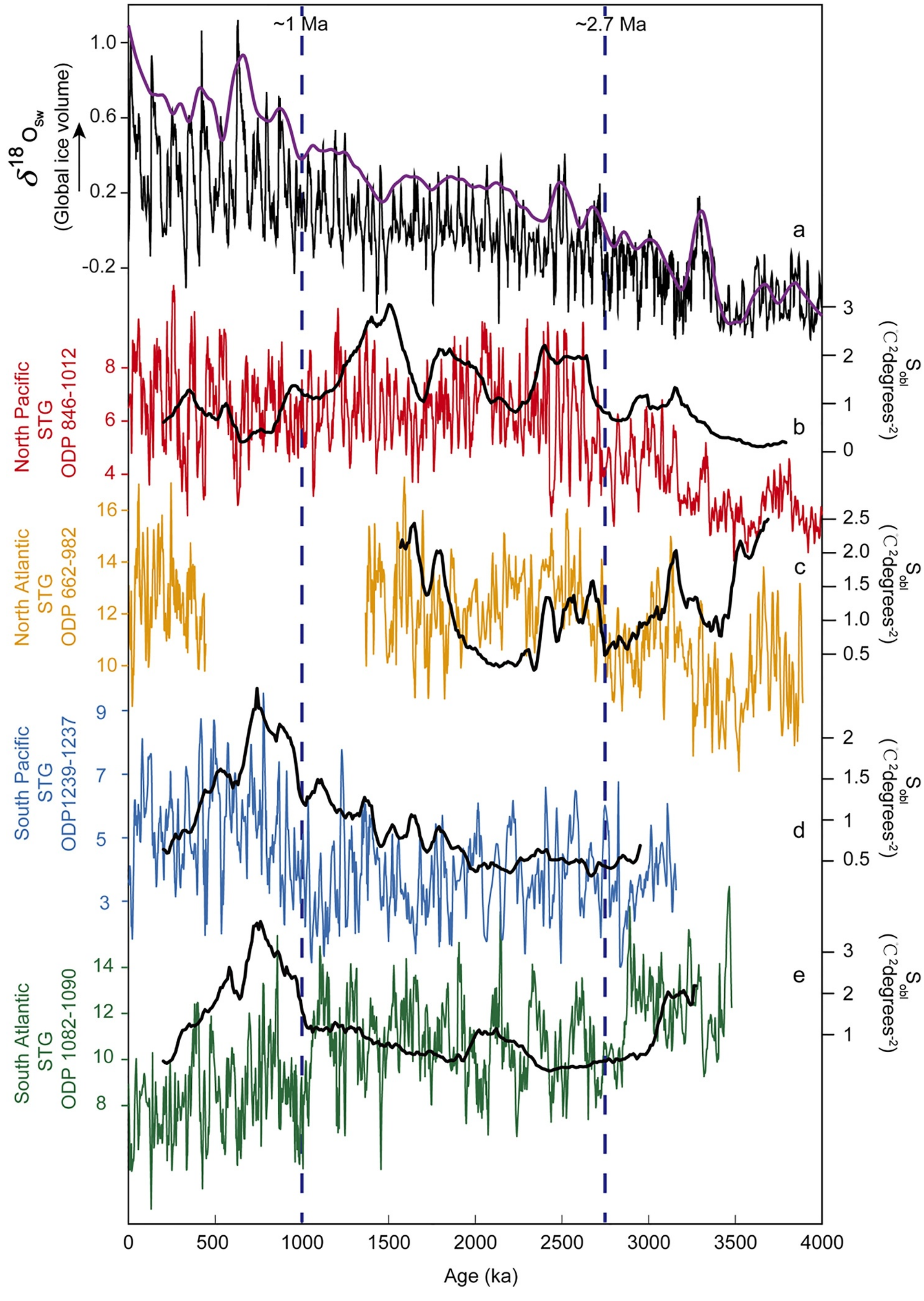


**Figure 6.** Meridional SST gradients (STG) and STG obliquity sensitivity ($S_{obl}$) for the North Atlantic, North Pacific, South Atlantic and South Pacific since 4 Ma. (a) Seawater $\delta^{18}O_{sw}$ (proxy for global ice volume; Rohling et al., 2021). The black arrow indicates increasing ice volume. (b) Meridional SST gradients between ocean drilling program (ODP) Sites 846 (3°S, 91°W; Lawrence et al., 2006; Liu & Herbert, 2004) and 1012 (32°N, 118°W; Brierley et al., 2009) for North Pacific and obliquity sensitivity ($S_{obl}$). (c) Meridional SST gradients between ODP Site 662 (1°S, 12°W; Herbert et al., 2010) and 982 (58°N, 16°W; Lawrence et al., 2009) for North Atlantic and obliquity sensitivity ($S_{obl}$). (d) Meridional SST gradients between ODP Sites 1239 (1°S, 82°W; Etourneau et al., 2010) and 1237 (16°S, 76°W; Dekens et al., 2007) for South Pacific and obliquity sensitivity ($S_{obl}$). (e) Meridional SST gradients between ODP Sites 1082 (21°S, 12°E; Etourneau et al., 2009) and 1090 (43°S, 9°E; Martínez-Garcia et al., 2010) for South Atlantic and obliquity sensitivity ($S_{obl}$). The thick black lines are $S_{obl.}$

25724525, 2024, 7, Downloaded from https://agupubs.onlinelibrary.wiley.com/doi/10.1029/2024PA004856 by University Of Southampton, Wiley Online Library on [25/07/2024]. See the Terms and Conditions (https://onlinelibrary.wiley.com/terms-and-conditions) on Wiley Online Library for rules of use; OA articles are governed by the applicable Creative Commons License

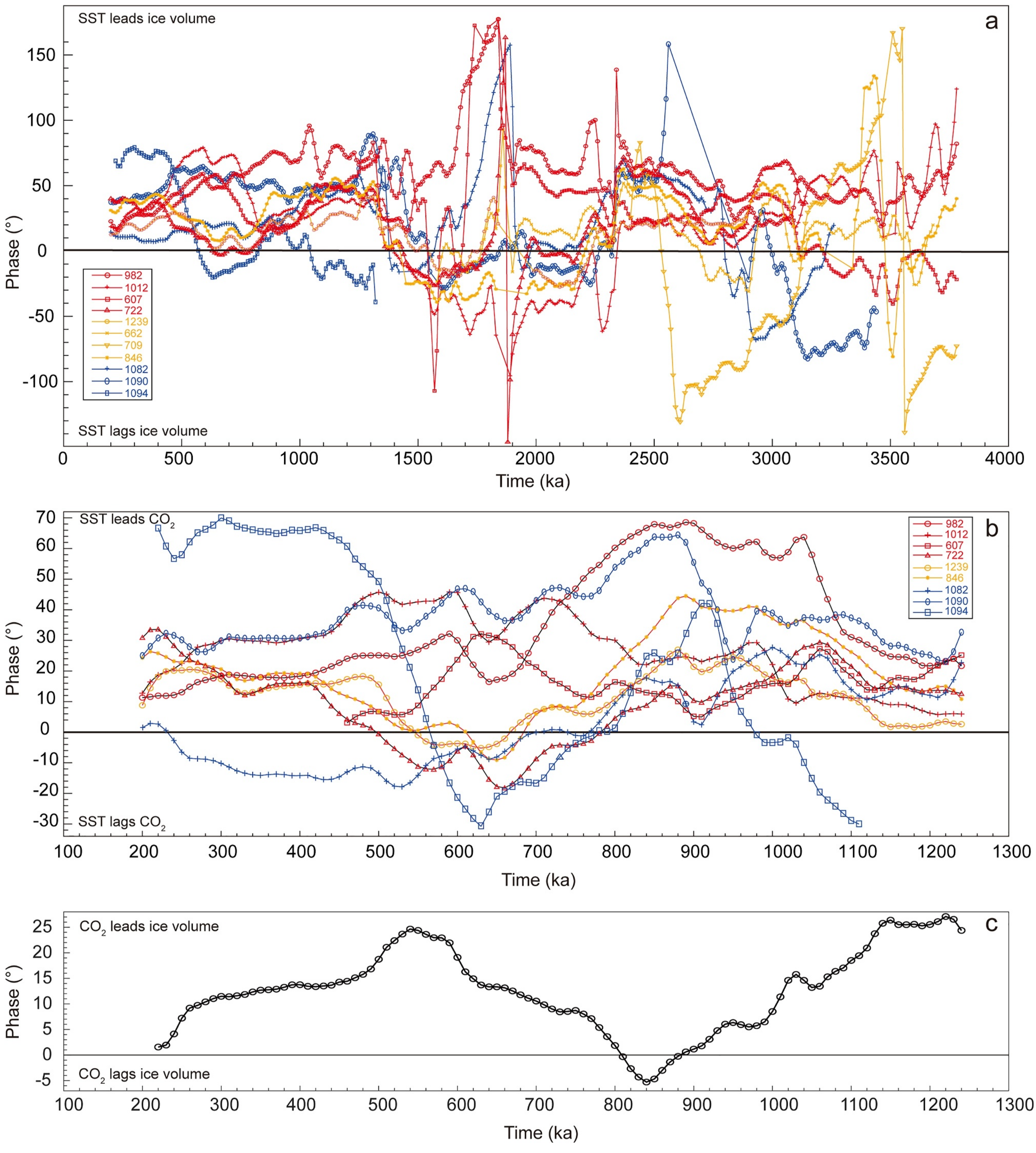


**Figure 7.** Phase analysis of SST-$\delta^{18}O_{sw}$ and SST-$CO_2$ concentrations at the 100-kyr eccentricity scale over the past 4 Ma. A typical confidence interval is ±6°. The $\delta^{18}O_{sw}$ data are from Rohling et al. (2021), atmospheric $CO_2$ concentrations are obtained from reconstruction based on leaf wax $\delta^{13}C$ at IODP Site U1446 (0–1.46 Ma; Yamamoto et al., 2022). Note that the red symbols and lines indicate SSTs in the NH, the green symbols and lines indicate SSTs in the equatorial regions, and the blue symbols and lines indicate SSTs in the SH. The time is based on the center of the window.

temperature gradient (Figures 6b and 6c), strengthening water vapor transport from the tropics (tropical Pacific and tropical Atlantic) to the Arctic (Brierley & Fedorov, 2010; Loutre et al., 2004) through the temperature-moisture feedback (Källén et al., 1979; Raymo & Nisancioglu, 2003). At the same time, NH high latitude cooling promotes Northern Hemisphere ice sheet development (Brierley & Fedorov, 2010; Lunt et al., 2008).



25724525, 2024, 7, Downloaded from https://agupubs.onlinelibrary.wiley.com/doi/10.1029/2024PA004856 by University Of Southampton, Wiley Online Library on [25/07/2024]. See the Terms and Conditions (https://onlinelibrary.wiley.com/terms-and-conditions) on Wiley Online Library for rules of use; OA articles are governed by the applicable Creative Commons License

High latitude cooling and increased sea ice cover cause intensification of water-column stratification (Sigman et al., 2004) and, thus, favor enhanced carbon accumulation in the deep-sea (Eggleston & Galbraith, 2018; Marinov et al., 2008; Odalen et al., 2018). In sum, oceanic processes associated with high-latitude SST reduction were crucial to atmospheric $CO_2$ reduction and NH glacial intensification during the Late Pliocene. This is supported by a substantial $S_{obl}$ increase for NH STG at ~2.7 Ma (Figures 6b and 6c). Several studies have proposed a simple inverse correlation between global mean surface temperature and STG measures, indicating a robust and fairly universal relationship through the past 10 million years (at low resolution) and the Eocene (on eccentricity time scales; Fokkema et al., 2024; Gaskell et al., 2022; Liu et al., 2022). Similarly, we find both a notable STG increase (Figures 6b–6d) and a distinct global SST decrease at ~2.7 Ma (Figures 2c–2m). The predictability of this relationship between global (sea) surface temperature and STG may be relevant to future climate change.

In contrast to the atmospheric $CO_2$ decrease from ~2.7 Ma, there is no notable long-term (>100 kyr) atmospheric $CO_2$ decrease after 1 Ma (Figure 2o), even though SST near Antarctica continued to decrease (ODP Site 1094). We note that Arctic SST (ODP Site 982) does not show this SST decrease. Inconsistent evolution of SST changes for the two poles gives a strong indication that global ice volume increases after 1 Ma had an important Antarctic component (Figure 2b). Mid-Pleistocene high latitude cooling may have caused persistent East Antarctic ice sheet expansion into the ocean so that it no longer contained an extensive terrestrial margin, which would favor in-phase variability of NH and SH ice sheets (Raymo et al., 2006). Ocean temperature plays an important role in controlling long-term fluctuations in ice sheet margins (Joughin et al., 2012), with marine-based ice particularly susceptible to rapid changes in ocean heat supply (Mengel & Levermann, 2014). Such mass balance sensitivity to ocean temperature has been emphasized for the EAIS (Hansen et al., 2015; Hasenfratz et al., 2019; McKay et al., 2012; Pollard & DeConto, 2009). Overall, therefore, we infer that EAIS variability may have become amplified from ~1 Ma by the development of an extensive marine ice sheet margin.

To test our argument about fundamental transitions in the relationships between SST, STG, and high-latitude ice sheets, we performed recurrence analyses of the NH and SH STG, as well as global ice volume ($\delta^{18}O_{sw}$). Results highlight major global ice volume shifts at ~2.7 and ~1 Ma (Figure 8a), consistent with previous studies that suggest a major global climate transition associated with high-latitude ice sheet development (Westerhold et al., 2020). Recurrence analyses of STG in the North Atlantic and North Pacific (ODP Sites 662–982 and 846–1012; Figures 8b and 8c) show a major shift at ~2.7 Ma, suggesting a link between NH STG and iNHG. Conversely, recurrence analyses of STG in the South Atlantic and South Pacific (Sites 1082–1090 and 1239–1237; Figures 8d and 8e) show a major transition at ~1 Ma, in agreement with the aforementioned concept of widespread marine EAIS margin development. The recurrence analyses, therefore, support our previous interpretations that there were two key climate transitions since 4 Ma (LP/EP and MPT) that contained critical involvement of SST and STG changes with distinctly different expressions (and, hence, governing processes) between the two hemispheres.

## 4. Conclusions

We compiled globally distributed SST records to investigate the involvement of orbital-scale SST trends and oceanic meridional temperature gradient changes in key climate transitions during the last 4 million years. We observe important orbital eccentricity and obliquity influences in the SST evolution, and infer both summer insolation and high-latitude ice volume (feedback) impacts on global SST. We find that the SST in the NH and the equatorial region shows a significant enhancement of the obliquity signal at ~2.7 Ma, and at the same time, the NH meridional SST gradient as well as its obliquity sensitivity also increases sharply at ~2.7 Ma. We infer that the enhancement of the obliquity signal in the NH and equatorial region during this period originates from large-scale NH ice sheet expansion. In addition, the increase in obliquity sensitivity of the southern hemisphere meridional SST gradient at ~1 Ma may be attributed to oceanward expansion of the Antarctic ice sheet margin. Phase analysis revealed key links between variations in SST, global ice volume, and atmospheric $CO_2$ levels, which underpinned the major climate shifts. Changes in SST can directly affect not only the formation and development of high-latitude ice sheets, but also global temperatures and thus ice volume by controlling changes in the atmospheric $CO_2$ concentration.



25724525, 2024, 7, Downloaded from https://agupubs.onlinelibrary.wiley.com/doi/10.1029/2024PA004856 by University Of Southampton, Wiley Online Library on [25/07/2024]. See the Terms and Conditions (https://onlinelibrary.wiley.com/terms-and-conditions) on Wiley Online Library for rules of use; OA articles are governed by the applicable Creative Commons License

10.1029/2024PA004856

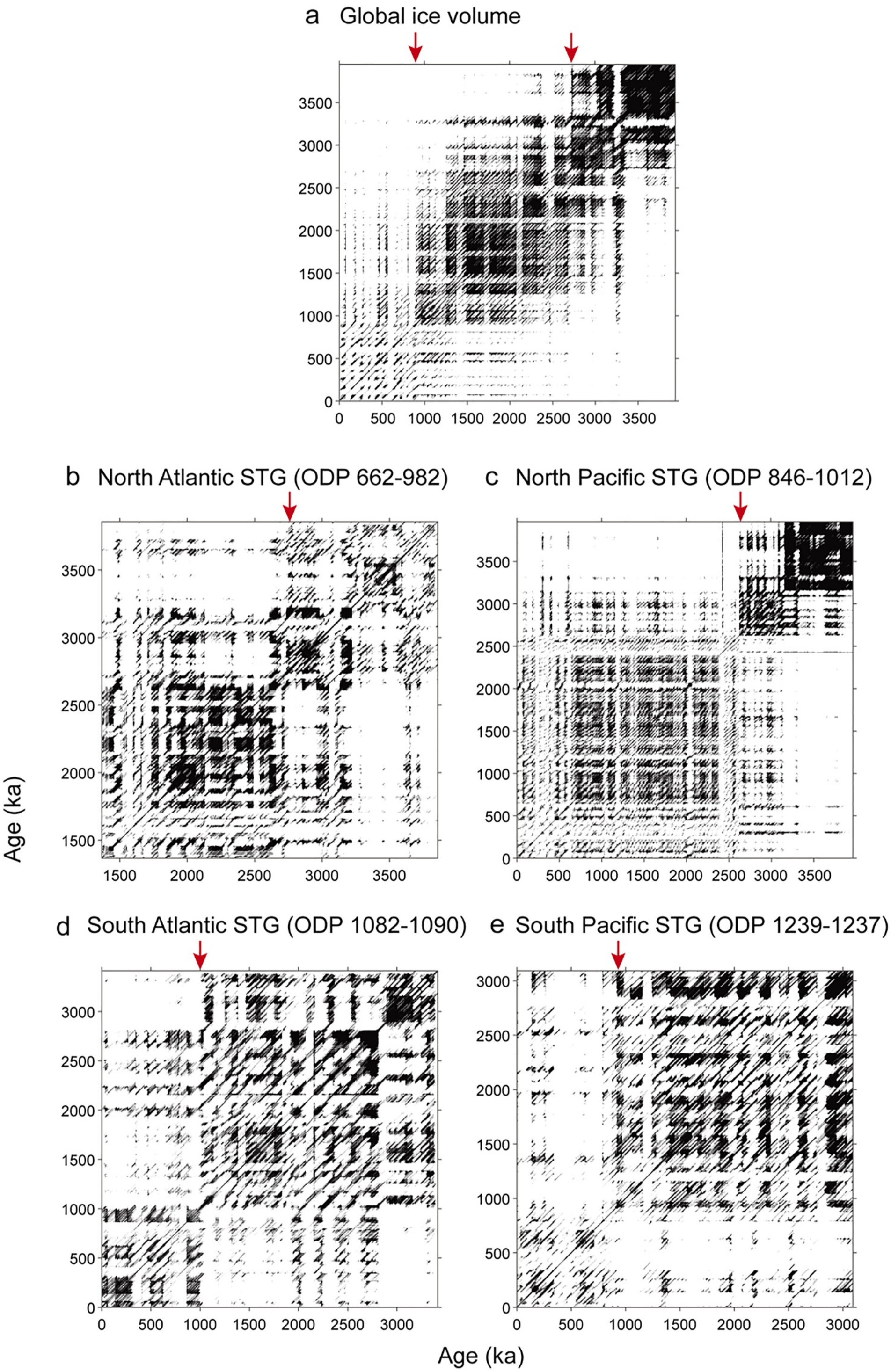


**Figure 8.** Recurrence plots of Global ice volume ($\delta^{18}O_{sw}$) and surface temperature gradients (STG) in the NH and SH. (a–e) Show recurrence plots of $\delta^{18}O_{sw}$ (global ice volume), STG in the North Atlantic, STG in the North Pacific, STG in the South Atlantic and STG in the South Pacific, respectively. The red arrows on top of the recurrence plots indicate points in time when transitions occurred. Transitions in these recurrence plots from darker areas to white areas indicate prominent systems changes (Marwan et al., 2007), see also Section 2.5 for further details. Global ice volume shows changes at ~2.7 and ~1 Ma. NH STG (ocean drilling program (ODP) 662–982; ODP 846–1012) show a change at ~2.7 Ma; SH STG (ODP 1239–1237; ODP 1082–1090) show a change at ~1 Ma. Note that subplot b has a different time axis than all the other subplots due to the lack of sea surface temperature data between ~1.5–0.5 Ma of ODP 662 in the North Atlantic.



25724525, 2024, 7, Downloaded from https://agupubs.onlinelibrary.wiley.com/doi/10.1029/2024PA004856 by University Of Southampton, Wiley Online Library on [25/07/2024]. See the Terms and Conditions (https://onlinelibrary.wiley.com/terms-and-conditions) on Wiley Online Library for rules of use; OA articles are governed by the applicable Creative Commons License

## Data Availability Statement

The SST data are available at Zhang (2024a). The data analysis was carried out in *R*. The complete codes reported in this study are available at Zhang (2024b).

**Acknowledgments**
This work was supported by the National Natural Science Foundation of China (Grant 42230208; 42172039; 42272033) and Postdoctoral Fellowship Program of CPSF (GZC20232471). EJR was supported by the Australian Centre for Excellence in Antarctic Science, an Australian Research Council Special Research Initiative (Project Number SR200100008).

## References

Anderson, R. F., Fleisher, M., Lao, Y., & Winckler, G. (2008). Modern $CaCO_3$ preservation in equatorial Pacific sediments in the context of late-Pleistocene glacial cycles. *Marine Chemistry*, *111*(1–2), 30–46. https://doi.org/10.1016/j.marchem.2007.11.011

Bartoli, G., Hönisch, B., & Zeebe, R. E. (2011). Atmospheric $CO_2$ decline during the Pliocene intensification of Northern hemisphere glaciations. *Paleoceanography*, *26*(4), PA4213. https://doi.org/10.1029/2010pa002055

Bosmans, J. H. C., Hilgen, F. J., Tuenter, E., & Lourens, L. J. (2015). Obliquity forcing of low-latitude climate. *Climate of the Past*, *11*(10), 1335–1346. https://doi.org/10.5194/cp-11-1335-2015

Brierley, C. M., & Fedorov, A. V. (2010). Relative importance of meridional and zonal sea surface temperature gradients for the onset of the ice ages and Pliocene-Pleistocene climate evolution. *Paleoceanography*, *25*(2), PA2214. https://doi.org/10.1029/2009pa001809

Brierley, C. M., Fedorov, A. V., Liu, Z., Herbert, T. D., Lawrence, K. T., & LaRiviere, J. P. (2009). Greatly expanded tropical warm pool and weakened Hadley circulation in the early Pliocene. *Science*, *323*(5922), 1714–1718. https://doi.org/10.1126/science.1167625

Callahan, J., Casey, R., Sharer, G., Templeton, M., & Trabant, C. (2018). IRISSeismic: Classes and methods for seismic data analysis. https://cran.r-project.org/web/packages/IRISSeismic/index.html

Cao, M. M., Wang, Z., Sui, Y., Li, Y., Zhang, Z., Xiao, A., et al. (2021). Mineral dust coupled with climate-carbon cycle on orbital timescales over the past 4 Ma. *Geophysical Research Letters*, *48*(18), e2021GL095327. https://doi.org/10.1029/2021gl095327

Cayan, D. R. (1992). Latent and sensible heat flux anomalies over the Northern oceans: Driving the sea surface temperature. *Journal of Physical Oceanography*, *22*(8), 859–881. https://doi.org/10.1175/1520-0485(1992)022<0859:lashfa>2.0.co;2

Chalk, T. B., Hain, M. P., Foster, G. L., Rohling, E. J., Sexton, P. F., Badger, M. P. S., et al. (2017). Causes of ice age intensification across the Mid-Pleistocene Transition. *Proceedings of the National Academy of Sciences of the United States of America*, *114*(50), 13114–13119. https://doi.org/10.1073/pnas.1702143114

Clark, P. U., Shakun, J. D., Rosenthal, Y., Köhler, P., & Bartlein, P. J. (2024). Global and regional temperature change over the past 4.5 million years. *Science*, *383*(6685), 884–890. https://doi.org/10.1126/science.adi1908

Clemens, S. C., & Tiedemann, R. (1997). Eccentricity forcing of Pliocene-early Pleistocene climate revealed in a marine oxygen-isotope record. *Nature*, *385*(6619), 801–804. https://doi.org/10.1038/385801a0

Clemens, S. C., Yamamoto, M., Thirumalai, K., Giosan, L., Richey, J. N., Nilsson-Kerr, K., et al. (2021). Remote and local drivers of Pleistocene South Asian summer monsoon precipitation: A test for future predictions. *Science Advances*, *7*(23), eabg3848. https://doi.org/10.1126/sciadv.abg3848

De Boer, A. M., & Hogg, A. M. (2014). Control of the glacial carbon budget by topographically induced mixing. *Geophysical Research Letters*, *41*(12), 4277–4284. https://doi.org/10.1002/2014gl059963

De Boer, B., Lourens, L. J., & van de Wal, R. S. W. (2014). Persistent 400,000-year variability of Antarctic ice volume and the carbon cycle is revealed throughout the Plio-Pleistocene. *Nature Communications*, *5*, 1–8. https://doi.org/10.1038/ncomms3999

Dekens, P. S., Ravelo, A. C., & McCarthy, M. D. (2007). Warm upwelling regions in the Pliocene warm period. *Paleoceanography*, *22*(3), PA3211. https://doi.org/10.1029/2006pa001394

Deser, C., Alexander, M. A., Xie, S. P., & Phillips, A. S. (2010). Sea surface temperature variability: Patterns and mechanisms. *Annual Review of Marine Science*, *2*(1), 115–143. https://doi.org/10.1146/annurev-marine-120408-151453

De Vleeschouwer, D., Drury, A. J., Vahlenkamp, M., Rochholz, F., Liebrand, D., & Pälike, H. (2020). High-latitude biomes and rock weathering mediate climate-carbon cycle feedbacks on eccentricity timescales. *Nature Communications*, *11*(1), 5013. https://doi.org/10.1038/s41467-020-18733-w

Dowsett, H. J., & Poore, R. Z. (1990). A new Planktic foraminifer transfer function for estimating Pliocene through Holocene sea surface temperatures. *Marine Micropaleontology*, *16*(1–2), 1–23. https://doi.org/10.1016/0377-8398(90)90026-i

Dowsett, H. J., Robinson, M. M., & Foley, K. M. (2009). Pliocene three-dimensional global ocean temperature reconstruction. *Climate of the Past*, *5*(4), 769–783. https://doi.org/10.5194/cp-5-769-2009

Eggleston, S., & Galbraith, E. D. (2018). The devil's in the disequilibrium: Multi-component analysis of dissolved carbon and oxygen changes under a broad range of forcings in a general circulation model. *Biogeosciences*, *15*(12), 3761–3777. https://doi.org/10.5194/bg-15-3761-2018

Etourneau, J., Martinez, P., Blanz, T., & Schneider, R. (2009). Pliocene-Pleistocene variability of upwelling activity, productivity, and nutrient cycling in the Benguela region. *Geology*, *37*(10), 871–874. https://doi.org/10.1130/g25733a.1

Etourneau, J., Schneider, R., Blanz, T., & Martinez, P. (2010). Intensification of the Walker and Hadley atmospheric circulations during the Pliocene-Pleistocene climate transition. *Earth and Planetary Science Letters*, *297*(1–2), 103–110. https://doi.org/10.1016/j.epsl.2010.06.010

Farmer, J. R., Hönisch, B., Haynes, L. L., Kroon, D., Jung, S., Ford, H. L., et al. (2019). Deep Atlantic Ocean carbon storage and the rise of 100,000-year glacial cycles. *Nature Geoscience*, *12*(5), 355–360. https://doi.org/10.1038/s41561-019-0334-6

Fedorov, A. V., Brierley, C. M., Lawrence, K. T., Liu, Z., Dekens, P. S., & Ravelo, A. C. (2013). Patterns and mechanisms of early Pliocene warmth. *Nature*, *496*(7443), 43–49. https://doi.org/10.1038/nature12003

Fedorov, A. V., Burls, N. J., Lawrence, K. T., & Peterson, L. C. (2015). Tightly linked zonal and meridional sea surface temperature gradients over the past five million years. *Nature Geoscience*, *8*(12), 975–980. https://doi.org/10.1038/ngeo2577

Fokkema, C. D., Agterhuis, T., Gerritsma, D., de Goeij, M., Liu, X., de Regt, P., et al. (2024). Polar amplification of orbital-scale climate variability in the early Eocene greenhouse world. *Climate of the Past*, *20*(6), 1303–1325. https://doi.org/10.5194/cp-20-1303-2024

Gaskell, D. E., Huber, M., O'Brien, C. L., Inglis, G. N., Acosta, R. P., Poulsen, C. J., & Hull, P. M. (2022). The latitudinal temperature gradient and its climate dependence as inferred from foraminiferal $\delta^{18}O$ over the past 95 million years. *Proceedings of the National Academy of Sciences of the United States of America*, *119*(11), e2111332119. https://doi.org/10.1073/pnas.2111332119

Hain, M. P., Sigman, D. M., & Haug, G. H. (2014). *The biological pump in the past. Reference module in Earth systems and environmental sciences, treatise on geochemistry* (2nd ed., Vol. 8, pp. 485–517). The Oceans and Marine Geochemistry.

Han, W. X., Appel, E., Galy, A., Rösler, W., Fang, X., Zhu, X., et al. (2020). Climate transition in the Asia inland at 0.8-0.6 Ma related to astronomically forced ice sheet expansion. *Quaternary Science Reviews*, *248*, 106580. https://doi.org/10.1016/j.quascirev.2020.106580

Hansen, M. A., Passchier, S., Khim, B., Song, B., & Williams, T. (2015). Threshold behavior of a marine-based sector of the East Antarctic Ice Sheet in response to early Pliocene ocean warming. *Paleoceanography*, *30*(6), 789–801. https://doi.org/10.1002/2014pa002704



25724525, 2024, 7, Downloaded from https://agupubs.onlinelibrary.wiley.com/doi/10.1029/2024PA004856 by University Of Southampton, Wiley Online Library on [25/07/2024]. See the Terms and Conditions (https://onlinelibrary.wiley.com/terms-and-conditions) on Wiley Online Library for rules of use; OA articles are governed by the applicable Creative Commons License

Hasenfratz, A. P., Jaccard, S. L., Martínez-García, A., Sigman, D. M., Hodell, D. A., Vance, D., et al. (2019). The residence time of Southern Ocean surface waters and the 100,000-year ice age cycle. *Science*, *363*(6431), 1080–1084. https://doi.org/10.1126/science.aat7067

Haug, G. H., Sigman, D. M., Tiedemann, R., Pedersen, T. F., & Sarnthein, M. (1999). Onset of permanent stratification in the subarctic Pacific Ocean. *Nature*, *401*(6755), 779–782. https://doi.org/10.1038/44550

Herbert, T. D., Peterson, L. C., Lawrence, K. T., & Liu, Z. (2010). Tropical ocean temperatures over the past 3.5 million years. *Science*, *328*(5985), 1530–1534. https://doi.org/10.1126/science.1185435

Hönisch, B., Hemming, N. G., Archer, D., Siddall, M., & McManus, J. F. (2009). Atmospheric carbon dioxide concentration across the Mid-Pleistocene transition. *Science*, *324*(5934), 1551–1554. https://doi.org/10.1126/science.1171477

IPCC. (2007). *Climate change 2007: The physical science basis. Contribution of working group I to the fourth assessment report of the inter-governmental panel on climate change*. Cambridge Univ. Press. 996.

Ito, T., & Follows, M. J. (2013). Air-sea disequilibrium of carbon dioxide enhances the biological carbon sequestration in the Southern Ocean. *Global Biogeochemical Cycles*, *27*(4), 1129–1138. https://doi.org/10.1002/2013gb004682

Jian, Z., Wang, Y., Dang, H., Lea, D. W., Liu, Z., Jin, H., & Yin, Y. (2020). Half-Precessional cycle of thermocline temperature in the Western equatorial Pacific and its Bihemispheric dynamics. *Proceedings of the National Academy of Sciences of the United States of America*, *117*(13), 7044–7051. https://doi.org/10.1073/pnas.1915510117

Joughin, I., Alley, R. B., & Holland, D. M. (2012). Ice-sheet response to oceanic forcing. *Science*, *338*(6111), 1172–1176. https://doi.org/10.1126/science.1226481

Jouzel, J., Masson-Delmotte, V., Cattani, O., Dreyfus, G., Falourd, S., Hoffmann, G., et al. (2007). Orbital and millennial Antarctic climate variability over the past 800,000 years. *Science*, *317*(5839), 793–796. https://doi.org/10.1126/science.1141038

Källén, E., Crafoord, C., & Ghil, M. (1979). Free oscillations in a climate model with ice-sheet dynamics. *Journal of the Atmospheric Sciences*, *36*(12), 2292–2303. https://doi.org/10.1175/1520-0469(1979)036<2292:foiacm>2.0.co;2

Karas, C., Nürnberg, D., Tiedemann, R., & Garbe-Schönberg, D. (2011). Pliocene Indonesian throughflow and Leeuwin current dynamics: Implications for Indian ocean polar heat flux. *Paleoceanography*, *26*(2), PA2217. https://doi.org/10.1029/2010pa001949

Kender, S., Ravelo, A. C., Worne, S., Swann, G. E. A., Leng, M. J., Asahi, H., et al. (2018). Closure of the Bering Strait caused mid-Pleistocene transition cooling. *Nature Communications*, *9*, 1–11. https://doi.org/10.1038/s41467-018-07828-0

Khatiwala, S., Schmittner, A., & Muglia, J. (2019). Air-sea disequilibrium enhances ocean carbon storage during glacial periods. *Science Advances*, *5*(6), eaaw4981. https://doi.org/10.1126/sciadv.aaw4981

Kohfeld, K. E., & Chase, Z. (2017). Temporal evolution of mechanisms controlling ocean carbon uptake during the last glacial cycle. *Earth and Planetary Science Letters*, *472*, 206–215. https://doi.org/10.1016/j.epsl.2017.05.015

Kohfeld, K. E., & Ridgwell, A. (2009). Glacial-interglacial variability in atmospheric $CO_2$. *Surface ocean-lower atmosphere processes*, *187*, 251–286. https://doi.org/10.1029/2008gm000845

Laskar, J., Robutel, P., Joutel, F., Gastineau, M., Correia, A. C. M., & Levrard, B. (2004). A long-term numerical solution for the insolation quantities of the Earth. *Astronomy and Astrophysics*, *428*(1), 261–285. https://doi.org/10.1051/0004-6361:20041335

Lawrence, K., Herbert, T. D., Brown, C. M., Raymo, M. E., & Haywood, A. M. (2009). High-amplitude variations in North Atlantic sea surface temperature during the early Pliocene warm period. *Paleoceanography*, *24*(2), PA2218. https://doi.org/10.1029/2008pa001669

Lawrence, K. T., Liu, Z., & Herbert, T. D. (2006). Evolution of the eastern tropical Pacific through Plio-Pleistocene glaciation. *Science*, *312*(5770), 79–83. https://doi.org/10.1126/science.1120395

Lawrence, K. T., Sosdian, S., White, H., & Rosenthal, Y. (2010). North Atlantic climate evolution through the Plio-Pleistocene climate transitions. *Earth and Planetary Science Letters*, *300*(3–4), 329–342. https://doi.org/10.1016/j.epsl.2010.10.013

Levy, R. H., Meyers, S. R., Naish, T. R., Golledge, N. R., McKay, R. M., Crampton, J. S., et al. (2019). Antarctic ice-sheet sensitivity to obliquity forcing enhanced through ocean connections. *Nature Geoscience*, *12*(2), 132–137. https://doi.org/10.1038/s41561-018-0284-4

Li, L., Li, Q., Tian, J., Wang, P., Wang, H., & Liu, Z. (2011). A 4-Ma record of thermal evolution in the tropical Western Pacific and its implications on climate change. *Earth and Planetary Science Letters*, *309*(1–2), 10–20. https://doi.org/10.1016/j.epsl.2011.04.016

Li, M. S., Hinnov, L., & Kump, L. (2019). Acycle: Time-series analysis software for paleoclimate research and education. *Computational Geosciences*, *127*, 12–22. https://doi.org/10.1016/j.cageo.2019.02.011

Li, T., Liu, F., Abels, H. A., You, C. F., Zhang, Z., Chen, J., et al. (2017). Continued obliquity pacing of East Asian summer precipitation after the mid-Pleistocene transition. *Earth and Planetary Science Letters*, *457*, 181–190. https://doi.org/10.1016/j.epsl.2016.09.045

Liebrand, D., de Bakker, A. T. M., Beddow, H. M., Wilson, P. A., Bohaty, S. M., Ruessink, G., et al. (2017). Evolution of the early Antarctic ice ages. *Proceedings of the National Academy of Sciences of the United States of America*, *114*(15), 3867–3872. https://doi.org/10.1073/pnas.1615440114

Lisiecki, L. E., & Raymo, M. E. A. (2005). Pliocene-Pleistocene stack of 57 globally distributed benthic $\delta^{18}O$ records. *Paleoceanography*, *20*(1), 1003. https://doi.org/10.1029/2004pa001071

Liu, X., Huber, M., Foster, G. L., Dessler, A., & Zhang, Y. G. (2022). Persistent high latitude amplification of the Pacific Ocean over the past 10 million years. *Nature Communications*, *13*(1), 7310. https://doi.org/10.1038/s41467-022-35011-z

Liu, Z. H., & Herbert, T. D. (2004). High-latitude influence on the eastern equatorial Pacific climate in the early Pleistocene epoch. *Nature*, *427*(6976), 720–723. https://doi.org/10.1038/nature02338

Lourens, L. J., Wehausen, R., & Brumsack, H. J. (2001). Geological constraints on tidal dissipation and dynamical Ellipticity of the Earth over the past three million years. *Nature*, *409*(6823), 1029–1033. https://doi.org/10.1038/35059062

Loutre, M. F., Paillard, D., Vimeux, F., & Cortijo, E. (2004). Does mean annual insolation have the potential to change the climate? *Earth and Planetary Science Letters*, *221*(1–4), 1–14. https://doi.org/10.1016/s0012-821x(04)00108-6

Lunt, D. J., Foster, G. L., Haywood, A. M., & Stone, E. J. (2008). Late Pliocene Greenland glaciation controlled by a decline in atmospheric $CO_2$ levels. *Nature*, *454*(7208), 1102–1105. https://doi.org/10.1038/nature07223

Marinov, I., Gnanadesikan, A., Sarmiento, J. L., Toggweiler, J. R., Follows, M., & Mignone, B. K. (2008). Impact of oceanic circulation on biological carbon storage in the ocean and atmospheric $pCO_2$. *Global Biogeochemical Cycles*, *22*(3), GB3007. https://doi.org/10.1029/2007gb002958

Martin, P., Archer, D., & Lea, D. W. (2005). Role of deep sea temperature in the carbon cycle during the last glacial. *Paleoceanography*, *20*(2), PA2015. https://doi.org/10.1029/2003pa000914

Martínez-Botí, M., Foster, G. L., Chalk, T. B., Rohling, E. J., Sexton, P. F., Lunt, D. J., et al. (2015). Plio-Pleistocene climate sensitivity evaluated us-ing high-resolution $CO_2$ records. *Nature*, *518*(7537), 49–54. https://doi.org/10.1038/nature14145

Martínez-Garcia, A., Rosell-Melé, A., Jaccard, S. L., Geibert, W., Sigman, D. M., & Haug, G. H. (2011). Southern Ocean dust-climate coupling over the past four million years. *Nature*, *476*(7360), 312–315. https://doi.org/10.1038/nature10310



25724525, 2024, 7, Downloaded from https://agupubs.onlinelibrary.wiley.com/doi/10.1029/2024PA004856 by University Of Southampton, Wiley Online Library on [25/07/2024]. See the Terms and Conditions (https://onlinelibrary.wiley.com/terms-and-conditions) on Wiley Online Library for rules of use; OA articles are governed by the applicable Creative Commons License

Martínez-Garcia, A., Rosell-Melé, A., McClymont, E. L., Gersonde, R., & Haug, G. H. (2010). Subpolar link to the emergence of the modern equatorial Pacific cold tongue. *Science*, *328*(5985), 1550–1553. https://doi.org/10.1126/science.1184480

Marwan, N. (2020). Cross recurrence plot Toolbox for MATLAB®, Ver. *5.22*. http://tocsy.pik-potsdam.de/CRPtoolbox/accessed2020-12-09

Marwan, N., Carmenromano, M., Thiel, M., & Kurths, J. (2007). Recurrence plots for the analysis of complex systems. *Physics Reports*, *438*(5–6), 237–329. https://doi.org/10.1016/j.physrep.2006.11.001

Max, L., Lembke-Jene, L., Zou, J., Shi, X., & Tiedemann, R. (2020). Evaluation of reconstructed sea surface temperatures based on $U^{K'}{}_{37}$ from sediment surface samples of the North Pacific. *Quaternary Science Reviews*, *243*, 106496. https://doi.org/10.1016/j.quascirev.2020.106496

McKay, R., Naish, T., Powell, R., Barrett, P., Scherer, R., Talarico, F., et al. (2012). Pleistocene variability of Antarctic ice sheet extent in the Ross embayment. *Quaternary Science Reviews*, *34*, 93–112. https://doi.org/10.1016/j.quascirev.2011.12.012

Mengel, M., & Levermann, A. (2014). Ice plug prevents irreversible discharge from East Antarctica. *Nature Climate Change*, *4*(6), 451–455. https://doi.org/10.1038/nclimate2226

Müller, P. J., Kirst, G., Ruhland, G., von Storch, I., & Rosell-Melé, A. (1998). Calibration of the Alkenone Paleotemperature index $U_{37}^{K'}$ based on core-tops from the eastern South Atlantic and the global ocean (60°N—60°S). *Geochimica et Cosmochimica Acta*, *62*(10), 1757–1772. https://doi.org/10.1016/s0016-7037(98)00097-0

Naish, T., Powell, R., Levy, R., Wilson, G., Scherer, R., Talarico, F., et al. (2009). Obliquity-paced Pliocene West Antarctic ice sheet oscillations. *Nature*, *458*(7236), 322–328. https://doi.org/10.1038/nature07867

O'Brien, C. L., Foster, G. L., Martínez-Botí, M. A., Abell, R., Rae, J. W. B., & Pancost, R. D. (2014). High sea surface temperatures in tropical warm pools during the Pliocene. *Nature Geoscience*, *7*(8), 606–611. https://doi.org/10.1038/ngeo2194

Odalen, M., Nycander, J., Oliver, K. I. C., Brodeau, L., & Ridgwell, A. (2018). The influence of the ocean circulation state on ocean carbon storage and $CO_2$ drawdown potential in an Earth system model. *Biogeosciences*, *15*(5), 1367–1393. https://doi.org/10.5194/bg-15-1367-2018

Pälike, H., Norris, R. D., Herrle, J. O., Wilson, P. A., Coxall, H. K., Lear, C. H., et al. (2006). The heartbeat of the Oligocene climate system. *Science*, *314*(5807), 1894–1898. https://doi.org/10.1126/science.1133822

Pena, L. D., & Goldstein, S. L. (2014). Thermohaline circulation crisis and impacts during the mid-Pleistocene transition. *Science*, *345*(6194), 318–322. https://doi.org/10.1126/science.1249770

Pollard, D., & DeConto, R. M. (2009). Modelling West Antarctic ice sheet growth and collapse through the past five million years. *Nature*, *458*(7236), 329–332. https://doi.org/10.1038/nature07809

Raymo, M. E., Lisiecki, L. E., & Nisancioglu, K. H. (2006). Plio-Pleistocene ice volume, Antarctic climate, and the global $\delta^{18}O$ record. *Science*, *313*(5786), 492–495. https://doi.org/10.1126/science.1123296

Raymo, M. E., & Nisancioglu, K. H. (2003). The 41 kyr world: Milankovitch's other unsolved mystery. *Paleoceanography*, *18*(1). https://doi.org/10.1029/2002pa000791

Ridgwell, A., & Zeebe, R. E. (2005). The role of the global carbonate cycle in the regulation and evolution of the Earth system. *Earth and Planetary Science Letters*, *234*(3–4), 299–315. https://doi.org/10.1016/j.epsl.2005.03.006

Rohling, E. J., Medina-Elizalde, M., Shepherd, J. G., Siddall, M., & Stanford, J. D. (2012). Sea surface and high-latitude temperature sensitivity to radiative forcing of climate over several glacial cycles. *Journal of Climate*, *25*(5), 1635–1656. https://doi.org/10.1175/2011jcli4078.1

Rohling, E. J., Yu, J., Heslop, D., Foster, G. L., Opdyke, B., & Roberts, A. P. (2021). Sea level and deep-sea temperature reconstructions suggest quasi-stable states and critical transitions over the past 40 million years. *Science Advances*, *7*(26), eabf5326. https://doi.org/10.1126/sciadv.abf5326

Rosell-Melé, A. (1998). Interhemispheric appraisal of the value of Alkenone indices as temperature and salinity proxies in high-latitude locations. *Paleoceanography*, *13*(6), 694–703. https://doi.org/10.1029/98pa02355

Samtleben, C., & Bickert, T. (1990). Coccoliths in sediment traps from the Norwegian Sea. *Marine Micropaleontology*, *16*(1–2), 39–64. https://doi.org/10.1016/0377-8398(90)90028-k

Sigman, D. M., Hain, M. P., & Haug, G. H. (2010). The polar ocean and glacial cycles in atmospheric $CO_2$ concentration. *Nature*, *466*(7302), 47–55. https://doi.org/10.1038/nature09149

Sigman, D. M., Jaccard, S., & Haug, G. H. (2004). Polar ocean stratification in a cold climate. *Nature*, *428*(6978), 59–63. https://doi.org/10.1038/nature02357

Smith, Y. M., Hill, D. J., Dolan, A. M., Haywood, A. M., Dowsett, H. J., & Risebrobakken, B. (2018). Icebergs in the Nordic seas throughout the late Pliocene. *Paleoceanography and Paleoclimatology*, *33*(3), 318–335. https://doi.org/10.1002/2017pa003240

Stap, L. B., de Boer, B., Ziegler, M., Bintanja, R., Lourens, L. J., & van de Wal, R. S. (2016). $CO_2$ over the past 5 million years: Continuous simulation and new $\delta^{11}B$-based proxy data. *Earth and Planetary Science Letters*, *439*, 1–10. https://doi.org/10.1016/j.epsl.2016.01.022

Tsutsui, H., Takahashi, K., Asahi, H., Jordan, R. W., Nishida, S., Nishiwaki, N., & Yamamoto, S. (2016). Nineteen-year time-series sediment trap study of Coccolithus Pelagicus and Emiliania Huxleyi (calcareous Nannoplankton) fluxes in the Bering Sea and subarctic Pacific Ocean. *Deep-Sea Research Part II Topical Studies in Oceanography*, *125*, 227–239. https://doi.org/10.1016/j.dsr2.2016.02.005

Wara, M. W., Ravelo, A. C., & Delaney, M. L. (2005). Permanent El Niño-like conditions during the Pliocene warm period. *Science*, *309*(5735), 758–761. https://doi.org/10.1126/science.1112596

Westerhold, T., Marwan, N., Drury, A. J., Liebrand, D., Agnini, C., Anagnostou, E., et al. (2020). An astronomically dated record of Earth's climate and its predictability over the last 66 million years. *Science*, *369*(6509), 1383–1387. https://doi.org/10.1126/science.aba6853

Willeit, M., Ganopolski, A., Calov, R., & Brovkin, V. (2019). Mid-Pleistocene transition in glacial cycles explained by declining $CO_2$ and regolith removal. *Science Advances*, *5*(4), eaav7337. https://doi.org/10.1126/sciadv.aav7337

Yamamoto, M., Clemens, S. C., Seki, O., Tsuchiya, Y., Huang, Y., O'ishi, R., & Abe-Ouchi, A. (2022). Increased interglacial atmospheric $CO_2$ levels followed the mid-Pleistocene Transition. *Nature Geoscience*, *15*(4), 307–313. https://doi.org/10.1038/s41561-022-00918-1

Yehudai, M., Kim, J., Pena, L. D., Jaume-Seguí, M., Knudson, K. P., Bolge, L., et al. (2021). Evidence for a Northern Hemisphere trigger of the 100,000-y glacial cyclicity. *Proceedings of the National Academy of Sciences of the United States of America*, *118*(46), e2020260118. https://doi.org/10.1073/pnas.2020260118

Yu, J., Anderson, R. F., Jin, Z., Menviel, L., Zhang, F., Ryerson, F. J., & Rohling, E. J. (2014). Deep South Atlantic carbonate chemistry and increased Interocean deep water exchange during last deglaciation. *Quaternary Science Reviews*, *90*, 80–89. https://doi.org/10.1016/j.quascirev.2014.02.018

Yu, J., Anderson, R. F., & Rohling, E. J. (2014). Deep Ocean carbonate chemistry and glacial-interglacial atmospheric $CO_2$ changes. *Oceanography*, *27*(1), 16–25. https://doi.org/10.5670/oceanog.2014.04

Yu, J., Menviel, L., Jin, Z., Thornalley, D., Barker, S., Marino, G., et al. (2016). Sequestration of carbon in the deep Atlantic during the last glaciation. *Nature Geoscience*, *9*(4), 319–324. https://doi.org/10.1038/ngeo2657

Yu, J., Menviel, L., Jin, Z. D., Anderson, R. F., Jian, Z., Piotrowski, A. M., et al. (2020). Last glacial atmospheric $CO_2$ decline due to widespread Pacific deep water expansion. *Nature Geoscience*, *13*(9), 628–633. https://doi.org/10.1038/s41561-020-0610-5



25724525, 2024, 7, Downloaded from https://agupubs.onlinelibrary.wiley.com/doi/10.1029/2024PA004856 by University Of Southampton, Wiley Online Library on [25/07/2024]. See the Terms and Conditions (https://onlinelibrary.wiley.com/terms-and-conditions) on Wiley Online Library for rules of use; OA articles are governed by the applicable Creative Commons License

Yu, J., Menviel, L., Jin, Z. D., Thornalley, D. J. R., Foster, G. L., Rohling, E. J., et al. (2019). More efficient North Atlantic carbon pump during the last glacial maximum. *Nature Communications*, *10*(1), 2170. https://doi.org/10.1038/s41467-019-10028-z

Zhang, Z. (2024a). Sea surface temperature data reconstructed by unsaturated alkenone index and foraminiferal Mg/Ca since 4 Ma. Version 2 [Dataset]. *ResearchData*, *4TU*. https://doi.org/10.4121/20486157

Zhang, Z. (2024b). Code for Obliquity sensitivity and phase analysis. Version 1 [Software]. *4TU. ResearchData*. https://doi.org/10.4121/2904d0f4-0f50-45f4-8363-69574ac1b2e5

## References From the Supporting Information

Eroglu, D., McRobie, F. H., Ozken, I., Stemler, T., Wyrwoll, K. H., Breitenbach, S. F. M., et al. (2016). See-saw relationship of the Holocene East Asian-Australian summer monsoon. *Nature Communications*, *7*(1), 12929. https://doi.org/10.1038/ncomms12929

Lüthi, D., Bereiter, B., Stauffer, B., Winkler, R., Schwander, J., Kindler, P., et al. (2010). $CO_2$ and $O_2/N_2$ variations in and just below the bubble–clathrate transformation zone of Antarctic ice cores. *Earth and Planetary Science Letters*, *297*(1–2), 226–233. https://doi.org/10.1016/j.epsl.2010.06.023

Schinkel, S., Dimigen, O., & Marwan, N. (2008). Selection of recurrence threshold for signal detection. *European Physical Journal Special Topics*, *164*(1), 45–53. https://doi.org/10.1140/epjst/e2008-00833-5

Dekens, P. S., Lea, D. W., Pak, D. K., & Spero, H. J. (2002). Core top calibration of Mg/Ca in tropical foraminifera: Refining Paleotemperature estimation. *Geochemistry, Geophysics, Geosystems*, *3*(4), 1–29. https://doi.org/10.1029/2001gc000200

Monnin, E., Indermühle, A., Dällenbach, A., Flückiger, J., Stauffer, B., Stocker, T. F., et al. (2001). Atmospheric $CO_2$ concentrations over the last glacial termination. *Science*, *291*(5501), 112–114. https://doi.org/10.1126/science.291.5501.112

Petit, J. R., Jouzel, J., Raynaud, D., Barkov, N. I., Barnola, J. M., Basile, I., et al. (1999). Climate and atmospheric history of the past 420,000 years from the Vostok ice core, Antarctica. *Nature*, *399*(6735), 429–436. https://doi.org/10.1038/20859

Pépin, L., Raynaud, D., Barnola, J., & Loutre, M. F. (2001). Hemispheric roles of climate forcings during glacial-interglacial transitions as deduced from the Vostok record and LLN-2D model experiments. *Journal of Geophysical Research*, *106*(D23), 31885–31892. https://doi.org/10.1029/2001jd900117

Raynaud, D., Barnola, J. M., Souchez, R., Lorrain, R., Petit, J. R., Duval, P., & Lipenkov, V. Y. (2005). The record for marine isotopic stage 11. *Nature*, *436*(7047), 39–40. https://doi.org/10.1038/43639b

Siegenthaler, U. R. S., Monnin, E., Kawamura, K., Spahni, R., Schwander, J., Stauffer, B., et al. (2005a). Supporting evidence from the EPICA Dronning Maud Land ice core for atmospheric $CO_2$ changes during the past millennium. *Tellus B: Chemical and Physical Meteorology*, *57*(1), 51–57. https://doi.org/10.1111/j.1600-0889.2005.00131.x

Siegenthaler, U., Stocker, T. F., Monnin, E., Lüthi, D., Schwander, J., Stauffer, B., et al. (2005b). Stable carbon cycle–climate relationship during the Late Pleistocene. *Science*, *310*(5752), 1313–1317. https://doi.org/10.1126/science.1120130

Vázquez Riveiros, N., Govin, A., Waelbroeck, C., Mackensen, A., Michel, E., Moreira, S., et al. (2016). Mg/Ca thermometry in Planktic foraminifera: Improving paleotemperature estimations for G. Bulloides and N. Pachyderma left. *Geochemistry, Geophysics, Geosystems*, *17*(4), 1249–1264. https://doi.org/10.1002/2015gc006234



25724525, 2024, 7, Downloaded from https://agupubs.onlinelibrary.wiley.com/doi/10.1029/2024PA004856 by University Of Southampton, Wiley Online Library on [25/07/2024]. See the Terms and Conditions (https://onlinelibrary.wiley.com/terms-and-conditions) on Wiley Online Library for rules of use; OA articles are governed by the applicable Creative Commons License